

---

# Towards Geometry-Aware Pareto Set Learning for Neural Multi-Objective Combinatorial Optimization

---

Yongfan Lu<sup>1</sup>, Zixiang Di<sup>1</sup>, Bingdong Li<sup>1✉</sup>, Shengcai Liu<sup>2</sup>, Hong Qian<sup>1</sup>, Peng Yang<sup>3</sup>,  
Ke Tang<sup>3</sup>, Aimin Zhou<sup>1</sup>

<sup>1</sup>East China Normal University

<sup>2</sup>Agency for Science, Technology and Research (A\*STAR)

<sup>3</sup>Southern University of Science and Technology  
51255901053@stu.ecnu.edu.cn, bdli@cs.ecnu.edu.cn

## Abstract

Multi-objective combinatorial optimization (MOCO) problems are prevalent in various real-world applications. Most existing neural MOCO methods rely on problem decomposition to transform an MOCO problem into a series of single-objective combinatorial optimization (SOCO) problems. However, these methods often approximate partial regions of the Pareto front and spend excessive time on diversity enhancement because of ambiguous decomposition and time-consuming precise hypervolume calculation. To address these limitations, we design a Geometry-Aware Pareto set Learning algorithm named GAPL, which provides a novel geometric perspective for neural MOCO via a Pareto attention model based on hypervolume expectation maximization. In addition, we propose a hypervolume residual update strategy to enable the Pareto attention model to capture both local and non-local information of the Pareto set/front. We also design a novel inference approach to further improve quality of the solution set and speed up hypervolume calculation. Experimental results on three classic MOCO problems demonstrate that our GAPL outperforms several state-of-the-art baselines via superior decomposition and efficient diversity enhancement.

## 1 Introduction

Multi-objective combinatorial optimization (MOCO) problems [1] are commonly seen in various fields, such as communication routing [2], logistics scheduling [3], etc. Typically, an MOCO problem requires the simultaneous optimization of multiple conflicting objectives, where the amelioration of an objective may lead to the deterioration of others. It is therefore desirable to discover a set of optimal solutions for MOCO problems, known as the Pareto optimal set [4]. Unfortunately, finding all the Pareto-optimal solutions of an MOCO problem is a challenging task, particularly considering that a single-objective combinatorial optimization (SOCO) problem might already be NP-hard.

Due to the exponentially increasing computational time required for exactly tackling MOCO problems [5], heuristic methods have been favored to yield an approximate Pareto set in practice over the past few decades. Although heuristic methods [6] are relatively efficient, they rely on domain-specific knowledge and involve massive iterative search. Recently, inspired by the success of deep reinforcement learning (DRL) in learning neural heuristics for solving SOCO problems, researchers have also explored DRL-based neural heuristics [7, 8] for MOCO problems. Typically, parameterized as a deep model, these neural heuristics adopt an end-to-end paradigm to construct solutions without iterative search, significantly reducing computational time compared with traditional heuristic methods.

Existing neural MOCO methods typically decompose an MOCO problem into a series of SOCO subproblems by aggregation functions and then solve them to obtain a Pareto set. This approach

can be seen as an extension of decomposition-based multi-objective optimization strategies [9] to an infinite preference scenario. However, previous methods suffer from several drawbacks. Firstly, there is a lack of clarity in interpreting the nature of aggregation functions for different subproblems (e.g. the integration of aggregation functions under various preferences). The assumption of equal importance for each preference causes the model to pay insufficient attention to difficult subproblems, which may cause the final solution set to approximate partial areas of the PF. The phenomenon easily leads to the decrease of solution set’s diversity (i.e. the adjacent subproblems correspond to duplicated solutions) due to the ignorance of mutual supportiveness of subproblems (e.g. consider the relationship between the current subproblem and the previous ones). Secondly, while there exists an algorithm [10] that introduced hypervolume into the reward to enhance diversity, the precise calculation of hypervolume is time-consuming and unaffordable due to its NP-hard nature [11].

After identifying the above-mentioned challenges, we have extended the idea of hypervolume expectation maximization [12, 13, 14] to MOCO. The contributions of this work can be summarized as follows: (1) We design a **Geometry-Aware Pareto set Learning**, termed as GAPL, which provides a geometric perspective for neural MOCO via a Pareto attention model. Mutual supportiveness of subproblems is the first to be leveraged to conduct geometry-adaptive learning for neural MOCO. (2) We propose a hypervolume residual update (HRU) strategy to make the Pareto attention model grasp both local and non-local information of the Pareto set/front and avoid being misled by weak solutions to a certain degree. (3) We design a novel inference approach named explicit and implicit dual inference (EI<sup>2</sup>) approach to improve the convergence and diversity of solutions. (4) Experimental results on three classic MOCO problems demonstrate that our GAPL outperforms state-of-the-art neural baselines by superior decomposition and efficient diversity enhancement.

## 2 Related work

**Exact and Heuristic Methods for MOCO.** Exact [15] and heuristic [6] algorithms are two groups of methods to solve MOCO problems in the past decades. The former can find all the Pareto-optimal solutions for only very small-scale problems, while the latter, commonly used in practical applications, can find the approximate Pareto-optimal solutions within a reasonable time. Many multi-objective evolutionary algorithms (MOEAs) are customized for MOCO, including NSGA-II [16], MOEA/D [9], and PPLS/D-C [17].

**Neural Heuristics for Combinatorial Optimization (CO).** In the literature, some end-to-end neural construction methods are developed for solving SOCO problems. The pioneering works [18, 19, 20] trained a pointer network to construct a near-optimal solution for SOCO problems. Kool et al. ([21]) proposed an attention model (AM) based on the transformer architecture. Another representative work is policy optimization with multiple optima (POMO) [22], which exploits the symmetry of solutions to further improve the performance of end-to-end models. Besides, the other line of works, known as neural improvement methods [23, 24], exploited DRL to assist the iterative improvement process from an initial solution, following a learn-to-improve paradigm.

**Neural Heuristics for MOCO.** Decomposition is a mainstream scheme in learning-based methods for multi-objective optimization [8, 25, 26]. Their basic idea is to decompose MOCO problems into multiple subproblems according to prescribed weight vectors, and then train a single model or multiple models to solve these subproblems. For example, Li et al. [7] and Zhang et al. [27] train multiple models collaboratively through a transfer learning strategy. Lin et al. ([8]) train a hypernetwork-based model to generate the decoder parameters conditioned on the preference for MOCO (PMOCO). Both MDRL [28] and EMNH [29] leverages meta-learning to train a deep reinforcement learning model that could be fine-tuned for various subproblems. NHDE [10] proposes indicator-enhanced DRL with an HGA model, which is the first to introduce the hypervolume into the reward for MOCO to enhance diversity.

**Hypervolume Expectation Maximization.** The hypervolume indicator measures the quality of MOCO solution sets and is consistent with Pareto dominance. Maximizing hypervolume is a basic principle in multiobjective optimization algorithm design [30, 31]. Many methods leverage hypervolume maximization to train neural networks. Deist et al. [32] adopt the idea of gradient search to obtain a finite set of Pareto solutions. Zhang et al. [14] extends hypervolume scalarization of a finite set [33] to hypervolume expectation with a simple MLP. However, in terms of sequential

prediction problems, traditional MLP is not suitable and the introduction of hypervolume expectation maximization needs to be further studied.

### 3 Preliminaries

#### 3.1 Multi-Objective Combinatorial Optimization

Without loss of generality, an MOCO problem can be mathematically stated as follows :

$$\begin{aligned} \min \mathbf{f}(\mathbf{x}) &= (f_1(\mathbf{x}), f_2(\mathbf{x}), \dots, f_m(\mathbf{x}))^T, \\ \text{s.t. } \mathbf{x} &\in \mathcal{X} \end{aligned} \quad (1)$$

where  $\mathbf{x} = (x_1, x_2, \dots, x_d)$  is the decision vector,  $\mathbf{f}(\cdot): \mathcal{X} \rightarrow \mathcal{T}$  is  $m$  objective functions,  $\mathcal{X}$  and  $\mathcal{T}$  denote the (nonempty) *decision space* and the *objective space*, respectively. Since the objectives are usually in conflict with each other, a set of trade-off solutions is to be sought. The concept of *Pareto optimality* is introduced.

**Definition 3.1 (Pareto dominance [4])** Given two solutions  $\mathbf{a}, \mathbf{b}$  in the region  $\mathcal{X}$ ,  $\mathbf{a}$  is said to dominate  $\mathbf{b}$  (denoted as  $\mathbf{a} \prec \mathbf{b}$ ) if and only if  $\forall i \in \{1, 2, \dots, m\}, f_i(\mathbf{a}) \leq f_i(\mathbf{b})$  and  $\exists j \in \{1, 2, \dots, m\}, f_j(\mathbf{a}) < f_j(\mathbf{b})$ .

**Definition 3.2 (Pareto optimality)** A solution  $\mathbf{a}^* \in \mathcal{X}$  is Pareto optimal if no other solution  $\mathbf{a} \in \mathcal{X}$  can dominate it.

**Definition 3.3 (Pareto Set and Pareto Front)** The solution set consisting of all the Pareto optimal solutions is called the Pareto set (PS):  $PS = \{\mathbf{a} \in \mathcal{X} | \forall \mathbf{b} \in \mathcal{X}, \mathbf{b} \not\prec \mathbf{a}\}$  and the corresponding objective vector set of the PS is the Pareto front (PF).

#### 3.2 Performance Evaluation

The nadir/ideal point of an MOCO problem is constructed by the worst/best objective values of the Pareto set  $y_i^{nadir} = \sup_{\mathbf{y} \in \mathcal{T}} \{y_i\}$  and  $y_i^{ideal} = \inf_{\mathbf{y} \in \mathcal{T}} \{y_i\}, \forall i \in 1, \dots, m$ . Given a set of objective vectors  $Y$ , the hypervolume (HV) indicator [34] is defined as follows,

$$\mathcal{HV}_r(Y) = \Lambda(\{\mathbf{q} \in \mathbb{R}^d | \exists \mathbf{p} \in Y : \mathbf{p} \preceq \mathbf{q} \text{ and } \mathbf{q} \preceq \mathbf{r}\}), \quad (2)$$

where  $\Lambda(\cdot)$  denotes the Lebesgue measure. and  $\mathbf{r}$  is a reference vector. We require that  $\mathbf{r} \succeq \mathbf{y}^{nadir}$ . All methods share the same reference point  $\mathbf{r}$  for a problem (see Appendix E).

## 4 Methodology

### 4.1 Overview

Our geometry-aware Pareto set learning (GAPL) introduces a novel geometric perspective based on hypervolume expectation maximization (HEM) for neural MOCO, providing a geometric mapping between preferences and solutions (Figure 1 and Algorithm 1). Moreover, we design a hypervolume residual update (HRU) strategy to better grasp local and non-local information and avoid the potential misleading caused by the unequal focus of different preferences. We also introduce an explicit and implicit dual inference (EI<sup>2</sup>) approach that enhances quality and efficiency, supported by local subset selection acceleration (LSSA).

### 4.2 Geometry Awareness via HEM

Pareto set learning (PSL) aims to learn the whole Pareto set by a model, which originated from traditional optimization [35]. Current neural MOCO methods tend to leverage weighted-sum (WS) or weighted-Tchebycheff (TCH) aggregation and/or use accurate HV to balance convergence (optimality) and diversity [8, 10]. However, they may overemphasize convergence or improve diversity at the sacrifice of high computational overhead. Thus, we propose a novel geometric view to formulate PSL based on hypervolume expectation maximization, which is only used with MLP in [14] before.

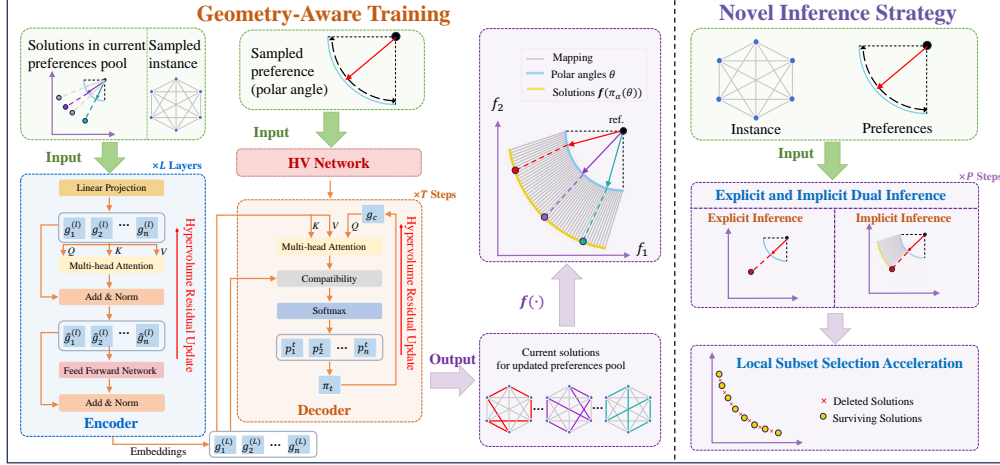


Figure 1: Pipeline of GAPL. **Left** ( $p'$ -th training iteration): GAPL is trained using a geometry-aware strategy to establish the mapping between preferences (polar angles) and solutions. Specifically, the encoder takes in a sampled instance and solutions generated from previous preferences  $\theta^{p-1}$ , which offers prior information for the current preference  $\theta$ . In addition,  $\theta$  generates the decoder parameters through a specifically designed HV network. The solutions derived from GAPL are aligned precisely with the polar angles in a polar coordinate system under mild conditions. **Right**: during inference, GAPL employs an explicit and implicit dual inference (EI<sup>2</sup>) approach to enhance convergence and diversity, and incorporates local subset selection acceleration (LSSA) to enhance efficiency. A well-trained Pareto attention model applies the EI<sup>2</sup> approach to each polar angle, resulting in solutions with superior convergence and diversity, while LSSA facilitates efficient selection.

Given a problem instance  $s$ , we sequentially solve its subproblem  $i \in \{1, \dots, P\}$ . The  $i$ -th subproblem is associated with weight polar angle  $\theta^i$ , which follows uniform distribution  $\text{Unif}(\Theta)$ :  $\Theta = [0, \frac{\pi}{2}]^{m-1}$ . Let  $\pi^i = (\pi_1^i, \dots, \pi_T^i)$  denotes the obtained solution at step  $i$ . Given a fully connected graph of  $T$  nodes (cities) with  $m$  cost objectives of an MOTSP instance,  $\pi$  denotes a tour that visits each city exactly once and returns to the starting node, and the objective functions are an  $m$ -dimensional vector  $\mathbf{y}(\pi) = (y_1(\pi), \dots, y_m(\pi))$ .

Here an HV scalarization function is introduced for unbiased estimation of the hypervolume indicator:

**Lemma 4.1 (Hypervolume scalarization of a finite set [33, 12, 13])**  $Y = \{\mathbf{y}^1, \dots, \mathbf{y}^n\}$  denotes set of finite objective vectors and  $\mathbf{r} = (r_1, \dots, r_m)$  denotes a reference point, which satisfies  $\forall i \in \{1, 2, \dots, m\}, \mathbf{r} \succ \mathbf{y}^i$ .

$$\mathcal{HV}_{\mathbf{r}}(Y) := \frac{\Phi}{m2^m} \mathbb{E}_{\theta}[(\max_{\mathbf{y} \in Y} \{\mathcal{G}^{mtch}(\mathbf{y}|\theta, \mathbf{r})\})^m] \quad (3)$$

$$\mathcal{G}^{mtch}(\mathbf{y}|\theta, \mathbf{r}) = \min_{i \in \{1, \dots, m\}} \{(r_i - y_i) / \lambda_i(\theta)\},$$

where  $\Phi = \frac{2\pi^{m/2}}{\Gamma(m/2)}$  denotes the area of the  $(m-1)$ -D unit sphere, which is a dimension-specific constant and  $\Gamma(x) = \int_0^{\infty} z^{x-1} e^{-z} dz$  denotes the analytic continuation of the factorial function.  $\boldsymbol{\lambda}(\theta) = (\lambda_1(\theta), \dots, \lambda_m(\theta))$  is the preference vector. It is the Cartesian coordinate of  $\theta$  on the positive unit sphere  $\mathbb{S}_+^{m-1}$ :  $\lambda_1(\theta) = \sin \theta_1 \sin \theta_2 \dots \sin \theta_{m-1}$ ,  $\lambda_2(\theta) = \sin \theta_1 \sin \theta_2 \dots \cos \theta_{m-1}$ ,  $\dots$ ,  $\lambda_m(\theta) = \cos \theta_1$ .

This scalarization function is a computationally-efficient and accurate estimator of the hypervolume that easily generalizes to higher dimensions. Moreover, it is polynomial in the number of objectives  $m$  when  $\mathcal{X}$  is suitably compact. This implies that the choice of scalarization functions and polar angles distribution  $\text{Unif}(\Theta)$  are theoretically sound and leads to provable convergence to the PF.

Given a set of uniform polar angles, accurately estimating HV with diminutive variance relies on numerous uniformly distributed solutions. However, solutions are not evenly distributed, especially in the nascent stage of optimization. Thus, it is necessary to build a mapping between the preferences

(polar angles) and the PS/PF, replacing the finite set  $Y$  via a Pareto attention model. In the other words, the Pareto attention model is able to predict nodes (cities) sequentially when given embedded preferences and further maps the node sequence from the instance space to the objective space. To sum up, what we need to realize is the mapping from preference space to objective space, with instance space as a “bridge”. Thus, we follow the idea of hypervolume expectation maximization [14] to construct our Pareto attention model. The detailed method of extending the scope of the input set in Lemma 4.1 to the PF containing an infinite number of objective vectors refers to Appendix F.

---

**Algorithm 1:** The training process of GAPL

---

**input** : preference distribution  $\Theta$ , instance distribution  $\mathcal{S}$ , number of training steps  $E$ , maximal size of polar angles pool  $P'$ , batch size  $B$ , instance size  $N$

**output** : The model parameter  $\beta$

- 1 Initialize the model parameters  $\beta$
- 2 **for**  $e = 1$  **to**  $E$  **do**
- 3      $s_i \sim \text{SampleInstance}(\mathcal{S}) \quad \forall i \in \{1, \dots, B\}$
- 4     Initialize  $\mathcal{F}_i^j \leftarrow \emptyset \quad \forall i, j \in \{1, \dots, N\}$
- 5     Initialize  $\theta^0 \leftarrow \emptyset$
- 6     **for**  $p' = 1$  **to**  $P'$  **do**
- 7          $\theta \sim \text{SamplePreference}(\Theta)$
- 8          $\theta^{p'} \leftarrow \theta^{p'-1} \cup \theta$
- 9          $\pi_i^j \sim \text{SampleSolution}(\text{Prob}_{\beta(\theta)}(\cdot | s_i, \theta), \mathcal{F}_i^j)$
- 10          $\mathcal{V}_\beta(\theta, s), \widetilde{\mathcal{H}\mathcal{V}_r}(\beta, \theta^{p'}, s) \leftarrow$  Calculate the projection distance and approximate HV by Eq. 10  $\forall i, j$
- 11          $\alpha_i^j \leftarrow$  Calculate expected HV improvement by Eq. 5  $\quad \forall i, j$
- 12          $R_i^j \leftarrow$  Calculate the reward by Eq. 4  $\quad \forall i, j$
- 13          $b_i \leftarrow \frac{1}{N} \sum_{j=1}^n (R_i^j) \quad \forall i$
- 14          $\nabla(J)(\beta) \leftarrow \frac{1}{Bn} \sum_{i=1}^B \sum_{j=1}^n [(-R_i^j - b_i) \nabla_{\beta(\theta)} \log \text{Prob}_{\beta(\theta)}(\pi_i^j | s_i, \theta, \mathcal{F}_i^j)] \quad \beta \leftarrow \text{Adam}(\beta, \nabla(J)(\beta))$
- 15          $\mathcal{F}_i^j \leftarrow \mathcal{F}_i^j \cup \{\mathbf{f}(\pi_i^j)\} \quad \forall i, j$
- 16     **end**
- 17 **end**
- 18 **end**

---

Based on the above discussion, it is favorable and feasible to take into account estimated hypervolume when training our Pareto attention model  $\Psi_\beta(\theta, s)$ . The update of the model will be discussed thoroughly in the next subsection. One remaining issue is how to generate the preference-conditioned parameters  $\beta_{\text{decoder}}(\theta)$ . We design an HV Network with reference to hypernetwork [36, 37, 38], which provides a powerful and efficient way for conditional computation and is widely used in transfer learning [39]. We use a simple MLP:  $\beta_{\text{decoder}}(\theta) = \text{MLP}(\lambda | \psi)$  to generate the decoder parameters conditioned on the polar angles, which is the first to take estimated HV into account. In view of this, our method can better capture the global characteristics of the PF. Moreover, our approximate calculation of hypervolume can better reduce time consumption and enhance model robustness. More details can be found in Appendix H. We also derive an alternative form of GAPL which uses the ideal point as a reference point and obtains interesting results in Appendix L.

### 4.3 Hypervolume Residual Update Strategy

Geometry awareness via hypervolume expectation maximization is based on the assumption of unequal importance for all subproblems. The assumption further requires the model to pay different attention to each subproblem. In order to enable the Pareto attention model to capture both local and non-local information of the Pareto set/front, we propose a hypervolume residual update (HRU) strategy to conduct more effective training. The reward function of subproblem  $i$  is defined as follows:

$$R_i = \omega \cdot \underbrace{\mathcal{V}_\beta(\theta^i, s)}_{\text{local}} + \alpha \cdot \underbrace{\widetilde{\mathcal{H}\mathcal{V}_r}(\beta, \theta^i, s)}_{\text{non-local}}. \quad (4)$$

Specifically, the reward function is composed of local and non-local terms: the projection distance of the  $i$ -th solution with respect to the polar angle  $\theta^i$  and the approximate hypervolume of all the selected solutions of subproblems 1 to  $i$ . The advantage of this combination is that it can balance exploration and exploitation. Each preference update will drive the evolution of the subsequent preferences. However, there is a deviation between the mapping solution of the Pareto attention model and the true solution with given preference and the deviation will decrease with the model training. Therefore, we introduce a local term decay parameter  $\omega$ , which is set to  $1 - \frac{ep}{EP}$ , where  $ep$  denotes the current epoch and  $EP$  denotes the total epochs since the local term is easier to learn than the non-local term. With the iteration of training epochs, our reward function will approach HV. During the training process, weak solutions may make the Pareto attention model misjudge the global information of the Pareto set/front. Based on the above considerations, we propose a novel definition, namely estimated hypervolume improvement (EHVI), which is as follows:

$$\mathbf{EHVI}(\beta, \theta^i, \boldsymbol{\theta}^i, s) = \widetilde{\mathcal{HV}}_r(\beta, \boldsymbol{\theta}^i, s) - \widetilde{\mathcal{HV}}_r(\beta, \boldsymbol{\theta}^i \setminus \{\theta^i\}, s). \quad (5)$$

When  $\mathbf{EHVI}(\cdot)$  is negative, we infer that the current polar angle  $\theta^i$  is mapped to a weak solution. In this case, the model will disregard the non-local term in order to avoid the weak solution from misleading the model. On the other hand, when  $\mathbf{EHVI}(\cdot)$  is positive, the non-local term is utilized to transfer valid global information to subsequent solutions. Regarding the above,  $\alpha = \lceil \mathbf{EHVI} \rceil$  since  $\widetilde{\mathcal{HV}}_r$  is a normalized value and then  $\mathbf{EHVI} \in (-1, 1)$ .

#### 4.4 Novel Inference Strategy

**Explicit and Implicit Dual Inference.** In the inference phase, for  $P$  given preferences, the well-trained model is used to sequentially solve  $P$  corresponding subproblems, as shown in Figure 1. In previous preference-conditioned inference approaches, each subproblem is treated separately, and the WS/TCH method is employed to determine the optimal solution. We refer to this approach as explicit inference, as it only considers the current preference directly, often resulting in local optima and producing duplicate solutions for similar preferences. To handle these issues, we design an additional implicit inference module, which aims to maximize  $\mathbf{EHVI}$  (Eq. 5). Specifically, we infer all the previous subproblems can provide valuable prior information and construct a partial approximate PF for HV estimation. The  $\mathbf{EHVI}$  serves as a suitable indicator to estimate the relevance and importance of the solution of the current preference based on all the previous preferences, effectively reducing duplicate solutions as  $\mathbf{EHVI}$  tends to zero in such a case. However, this approach may also carry the risk of local optima, as the distribution of subsequent preferences and solutions is unknown. To mitigate this, we propose the explicit and implicit dual inference (EI<sup>2</sup>) approach to enable the cooperation of both inference strategies, thereby facilitating better approximation of the PS/PF.

**Local Subset Selection Acceleration.** After the EI<sup>2</sup> approach, several solutions with superior convergence and diversity are obtained. Then, we want to obtain the optimal subset with a given size restriction (usually  $P$ ). However, traditional local subset selection is time-consuming and unaffordable. In view of this, we introduce local subset selection acceleration (LSSA) from [40] to improve efficiency.

LSSA is based on potential energy from the physics domain. The potential energy of a system  $Q$  is defined as follows:

$$E(Q) = \sum_{\mathbf{x}^i \in Q} \sum_{\mathbf{x}^j \in P \setminus \mathbf{x}^i} U(\mathbf{x}^i, \mathbf{x}^j), \quad U(\mathbf{x}^i, \mathbf{x}^j) = \frac{1}{\|\mathbf{x}^i - \mathbf{x}^j\|^c}, \quad (6)$$

where  $\|\cdot\|$  denotes the module and  $c$  is a control parameter. The time complexity of a potential energy calculation for a system  $Q$  is  $O(n_1^2 m)$ . Suppose there are  $k$  iterations on average for a local subset selection (LSS), the overall time complexity in terms of potential energy calculation is  $O(n_1^4 m k)$ , where  $n_1$  and  $m$  denote the size of  $Q$  and objective dimensions of each solution, respectively.

Since the overall time complexity is too high, an acceleration strategy is adopted by using the properties of both optimization and the potential energy function. Let  $Q_1$  contain current selected solutions while  $Q_2$  contains the unselected ones. The contribution of a selected one  $e1(\mathbf{x})$  and an unselected one  $e2(\mathbf{x})$  to  $Q_1$  can be defined by  $e1(\mathbf{x}) = \sum_{\mathbf{y} \in Q_1 \setminus \mathbf{x}} U(\mathbf{x}, \mathbf{y})$ ,  $e2(\mathbf{x}) = \sum_{\mathbf{y} \in Q_2} U(\mathbf{x}, \mathbf{y})$ . Thus,  $E(Q_1)$  (Eq. 6) is equivalent to  $\sum_{\mathbf{x} \in Q_1} e1(\mathbf{x})$ . Consider one of  $Q_1$ 's neighbors  $Q_1 \setminus \{\mathbf{x}\} \cup \{\mathbf{y}\}$ , where  $\mathbf{x} \in Q_1$  and  $\mathbf{y} \in Q_2$ . Instead of the time-consuming calculation of Eq. 6, we can obtain the

difference between the energy values of the two systems by LSSA strategy to calculate the energy of a new system with high efficiency:

$$\Delta E(Q_1) = e1(\mathbf{x}) - e2(\mathbf{y}) + U(\mathbf{x}, \mathbf{y}). \quad (7)$$

In the same way, we can also store the contributions difference of all the selected and unselected solutions in the running process. The time complexity to update  $E(Q_1)$  is  $O(1)$ . Moreover, if all  $U(\mathbf{x}, \mathbf{y})$  are preprocessed, the time complexity of LSS reduces from  $O(n_1^4mk)$  to  $O(n_1^2m + n_1^2k)$ . LSSA strategy can find the optimal subset from the solutions selected by EI<sup>2</sup> with high efficiency. All details and proofs are provided in Appendix G.

## 5 Experimental Study

**Problems.** We conducted comprehensive experiments to evaluate GAPL on three typical MOCO problems that are commonly studied in the neural MOCO field [7, 8], namely multi-objective traveling salesman problem (MOTSP) [41], multi-objective capacitated vehicle routing problem (MOCVRP) [42], and multi-objective knapsack problem (MOKP) [43]. Following the convention in [8, 10], we consider the instances with different sizes, i.e.  $T = 20/50/100$  for bi-objective TSP (Bi-TSP), tri-objective TSP (Tri-TSP) and bi-objective CVRP (Bi-CVRP), and  $T = 50/100/200$  for bi-objective KP (Bi-KP).

**Hyperparameters.** We randomly generated 5000 problem instances on the fly in each epoch for training GAPL. The optimizer is ADAM with learning rate  $\eta = 10^{-4}$  and weight decay  $10^{-6}$  for 200 epochs. During training, the maximal size of polar angles pool  $P'$  is set to 20 for each instance. During inference, we generate  $P = 101$  and  $P = 10201$  uniformly distributed preferences (polar angles) for  $m = 2$  and  $m = 3$ , respectively. Besides, we set the control parameter  $c$  to  $2m$  and set  $N$  to  $T$ , following [22]. All hyperparameter studies can be found in Appendix M.3.

**Baselines.** We compare GAPL with two kinds of state-of-the-art baselines: 1) Traditional heuristics. We introduce a widely-used evolutionary algorithm for MOCO: NSGAII [16] is a Pareto dominance-based multiobjective genetic algorithm; LKH [44] and dynamic programming (DP) are employed to solve the weighted-sum (WS) based subproblems for MOTSP and MOKP, denoted as WS-LKH and WS-DP, respectively; PPLS/D-C [17] is a specialized MOEA for MOCO with local search techniques. 2) Neural heuristics. DRL-MOA [7] decomposes a MOCO with different preferences and builds a Pointer Network [20] to solve each subproblem; PMOCO [8] is the first to train a single model for all different preferences simultaneously. NHDE-P [10] proposes an indicator-enhanced deep reinforcement learning method to guide the model, which is the first to take the diversity into consideration in the reward. EMNH [10] leverages meta-learning to train a DRL model that could be fine-tuned for various subproblems.

**Metrics.** Hypervolume (HV) [45] is used for performance evaluation, where a higher HV means a better solution set. The average HV, gaps with respect to GAPL, and total running time for 200 random test instances are reported. The best (second-best) results are highlighted in **bold** (underline). All the compared methods share the same reference points (see Appendix E).

### 5.1 Results and Analysis

The overall comparison results are recorded in Table 1, including the average HV, gap, and total running time for 200 random test instances. Given the same number of preferences, GAPL significantly surpasses PMOCO and NHDE-P across all problems and sizes. When instance augmentation (aug.) is equipped, GAPL achieves the smallest gap among the methods on most cases except Bi-CVRP100 where DRL-MOA performs better. However, DRL-MOA incurs significantly more training time overhead to prepare multiple models for different weights. Besides, DRL-MOA exhibits significant advantages on problems with extremely imbalanced scales (i.e. Bi-CVRP), as it can more effectively decompose subproblems by utilizing prior information. This advantage becomes more pronounced on instances with larger sizes. In contrast, preference-conditioned methods rely on uniform acquisition of preferences. Anyway, GAPL shows superior performance than all the other preference-conditioned methods (e.g. PMOCO and NHDE-P) via its geometric adaptation on

Table 1: Experimental results on 200 random instances for MOCO problems.

Method	Bi-TSP20			Bi-TSP50			Bi-TSP100		
	HV $\uparrow$	Gap $\downarrow$	Time $\downarrow$	HV $\uparrow$	Gap $\downarrow$	Time $\downarrow$	HV $\uparrow$	Gap $\downarrow$	Time $\downarrow$
WS-LKH (101 pref.)	0.6268	1.10%	4.2m	0.6401	0.55%	41m	0.7071	0.10%	2.6h
PPLS/D-C (200 iter.)	0.6256	1.29%	25m	0.6282	2.40%	2.7h	0.6845	3.30%	1.1h
NSGAII-TSP	0.5941	6.26%	40m	0.5984	7.03%	43m	0.6643	6.15%	53m
DRL-MOA (101 models)	0.6257	1.28%	7s	0.6360	1.18%	10s	0.6971	1.51%	22s
PMOCO (101 pref.)	0.6266	1.14%	8s	0.6349	1.35%	13s	0.6953	1.77%	21s
NHDE-P (101 pref.)	0.6288	0.79%	4.3m	0.6389	0.73%	8.3m	0.7005	1.03%	16m
GAPL (101 pref.)	<u>0.6324</u>	<u>0.24%</u>	18s	0.6404	0.53%	23s	0.7014	0.89%	31s
EMNH (aug.)	0.6271	1.05%	1.3m	0.6408	0.44%	4.6m	0.7023	0.78%	17m
PMOCO (101 pref. & aug.)	0.6273	1.03%	46s	0.6392	0.69%	3.1m	0.6997	1.14%	5.7m
NHDE-P (101 pref. & aug.)	0.6296	0.66%	9.8m	<u>0.6429</u>	<u>0.09%</u>	19m	0.7050	0.40%	40m
GAPL (101 pref. & aug.)	<b>0.6340</b>	<b>0.00%</b>	1.2m	<b>0.6437</b>	<b>0.00%</b>	4.5m	<b>0.7079</b>	<b>0.00%</b>	6.8m
Method	Bi-CVRP20			Bi-CVRP50			Bi-CVRP100		
PPLS/D-C (200 iter.)	0.3351	4.04%	1.2h	0.4149	3.42%	9.6h	0.4083	1.87%	37h
NSGAII-CVRP	0.3123	10.57%	37m	0.3631	15.48%	38m	0.3538	14.97%	43m
DRL-MOA (101 models)	0.3453	1.12%	7s	0.4270	0.61%	20s	<b>0.4176</b>	<b>-0.36%</b>	40s
PMOCO (101 pref.)	0.3467	0.72%	8s	0.4271	0.58%	18s	0.4131	0.72%	36s
NHDE-P (101 pref.)	0.3458	0.97%	1.5m	0.4248	1.12%	3.1m	0.4127	0.82%	5.3m
GAPL (101 pref.)	0.3471	0.63%	17s	0.4279	0.47%	31s	0.4143	0.43%	58s
EMNH (aug.)	0.3471	0.60%	33s	0.4250	1.07%	1.4m	0.4146	0.36%	3.7m
PMOCO (101 pref. & aug.)	<u>0.3481</u>	<u>0.32%</u>	1m	<u>0.4287</u>	<u>0.21%</u>	2.1m	0.4150	0.26%	4.5m
NHDE-P (101 pref. & aug.)	0.3465	0.77%	5.1m	0.4262	0.79%	9.2m	0.4139	0.53%	21m
GAPL (101 pref. & aug.)	<b>0.3492</b>	<b>0.00%</b>	2.2m	<b>0.4297</b>	<b>0.00%</b>	4.1m	<u>0.4161</u>	<u>0.00%</u>	6.8m
Method	Bi-KP50			Bi-KP100			Bi-KP200		
WS-DP (101 pref.)	0.3563	0.50%	9.5m	0.4531	0.77%	1.2h	0.3599	2.04%	3.7h
PPLS/D-C (200 iter.)	0.3528	1.48%	18m	0.4480	1.88%	46m	0.3541	3.62%	1.4h
NSGAII-KP	0.3112	13.10%	30m	0.3514	23.07%	31m	0.3511	4.44%	33m
EMNH	0.3561	0.56%	17s	0.4535	0.68%	53s	0.3603	1.93%	2.3m
DRL-MOA (101 models)	0.3559	0.61%	8s	0.4531	0.77%	13s	0.3601	1.99%	1.1m
PMOCO (101 pref.)	0.3552	0.81%	13s	0.4522	0.96%	19s	0.3595	2.15%	50s
NHDE-P (101 pref.)	<u>0.3564</u>	<u>0.47%</u>	1.1m	0.4541	<u>0.55%</u>	2.5m	<u>0.3612</u>	<u>1.69%</u>	5.3m
GAPL (101 pref.)	<b>0.3582</b>	<b>0.00%</b>	21s	<b>0.4571</b>	<b>0.00%</b>	33s	<b>0.3674</b>	<b>0.00%</b>	1.4m
Method	Tri-TSP20			Tri-TSP50			Tri-TSP100		
WS-LKH (210 pref.)	0.4718	1.50%	20m	0.4493	2.50%	3.3h	0.5160	1.28%	1.1h
PPLS/D-C (200 iter.)	0.4698	1.92%	1.3h	0.4174	9.42%	3.8h	0.4376	16.28%	1.3h
NSGAII-TSP	0.4216	11.98%	2.1h	0.4130	10.37%	2.3h	0.4291	17.91%	2.5h
DRL-MOA (1035 models)	0.4712	1.63%	51s	0.4396	4.60%	1.5s	0.4915	5.97%	3.1s
PMOCO (10201 pref.)	0.4749	0.86%	8.9m	0.4489	2.58%	17m	0.5102	2.39%	34m
NHDE-P (10201 pref.)	0.4764	0.54%	53m	0.4513	2.06%	1.8h	0.5118	2.09%	4.3h
GAPL (10201 pref.)	0.4782	0.19%	10m	0.4531	1.71%	19m	0.5129	1.87%	41m
EMNH (aug.)	0.4712	1.63%	7.1m	0.4418	4.12%	58m	0.4973	4.86%	2.4h
PMOCO (10201 pref. & aug.)	0.4757	0.69%	20m	0.4573	0.76%	1.1h	0.5123	1.99%	4.3h
NHDE-P (10201 pref. & aug.)	<u>0.4772</u>	<u>0.38%</u>	2.1h	<u>0.4595</u>	<u>0.28%</u>	6.7h	<u>0.5210</u>	<u>0.33%</u>	15.3h
GAPL (10201 pref. & aug.)	<b>0.4791</b>	<b>0.00%</b>	26m	<b>0.4609</b>	<b>0.00%</b>	1.3h	<b>0.5227</b>	<b>0.00%</b>	4.8h

Bi-CVRP100. Finally, we believe that GAPL has the potential to be further improved by incorporating additional prior information.

Regarding the inference efficiency, GAPL generally requires slightly more time compared with PMOCO due to the utilization of LSSA. However, the LSSA demonstrates a notable characteristic of time complexity that remains unaffected by the number of instance nodes, resulting in high efficiency even for larger instances. Furthermore, the time consumption of GAPL is significantly lower than that of NHDE-P, since NHDE-P adopts accurate HV calculation and multiple Pareto optima strategy. This is also observed during the training process.

## 5.2 Ablation Study

To analyze the effect of the HRU strategy, we compare GAPL with 4 variants: GAPL without non-local term (GAPL w/o non-local), GAPL without local term (GAPL w/o local), GAPL with a constant of  $\alpha = 1$  (GAPL w/o residual) and GAPL without local term decay parameter (GAPL w/o local decay). Moreover, we compare GAPL with GAPL without implicit inference (GAPL w/o



implicit) and GAPL without explicit inference (GAPL w/o explicit), to study the  $EI^2$  approach. As seen in Table 2. The performance of GAPL is impaired when any of the components is ablated. Besides, both local and non-local terms are critical for model training since their absence leads to the top 2 biggest gaps. The introduction of adaptive parameters  $\omega$  and  $\alpha$  can effectively control the focus of the Pareto attention model to make the reward function approach HV. We also show the inference time of GAPL and GAPL w/o LSSA in Figure 2. GAPL w/o LSSA adopts traditional LSS. It is evident that LSSA can improve efficiency, as discussed in Section 4.4.

Table 2: Effects of HRU strategy and  $EI^2$  approach.

Method	Bi-TSP50		Bi-CVRP50		Bi-KP100		Tri-TSP50	
	HV $\uparrow$	Gap $\downarrow$	HV $\uparrow$	Gap $\downarrow$	HV $\uparrow$	Gap $\downarrow$	HV $\uparrow$	Gap $\downarrow$
GAPL w/o non-local	0.6347	0.86%	0.4368	0.03%	0.4521	0.12%	0.4487	0.95%
GAPL w/o local	0.6251	2.35%	0.4239	3.14%	0.4416	3.31%	0.4326	4.51%
GAPL w/o residual	0.6379	0.36%	0.4361	0.36%	0.4547	0.06%	0.4507	0.07%
GAPL w/o local decay	<b>0.6401</b>	<b>0.03%</b>	<b>0.4376</b>	<b>0.04%</b>	<b>0.4566</b>	<b>0.02%</b>	<b>0.4529</b>	<b>0.02%</b>
GAPL w/o implicit	0.6371	0.48%	0.4367	0.04%	0.4558	0.04%	0.4517	0.05%
GAPL w/o explicit	0.6363	0.61%	0.4348	0.08%	0.4549	0.06%	0.4511	0.06%
GAPL	<b>0.6404</b>	<b>0.00%</b>	<b>0.4379</b>	<b>0.00%</b>	<b>0.4571</b>	<b>0.00%</b>	<b>0.4531</b>	<b>0.00%</b>

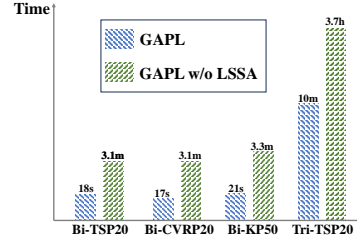


Figure 2: The time consumed by GAPL and GAPL w/o LSSA.

### 5.3 Validity of Geometric Adaptation

As demonstrated earlier, GAPL aims to interpret the nature of aggregation functions for different subproblems and understand their interconnections. In GAPL, the integration of mappings between polar angles (preferences) and solutions approximates the HV. This allows the Pareto attention model to effectively capture these mappings, benefiting from its larger state space compared with traditional heuristic optimization methods. Furthermore, GAPL improves previous decomposition-based approaches by building the assumption of unequal importance for all subproblems. As a result, GAPL is able to approximate the entire Pareto front and prevent duplicate solutions across different subproblems. Figure 3 visualizes the mapping of GAPL and other decomposition-based methods in the objective space.

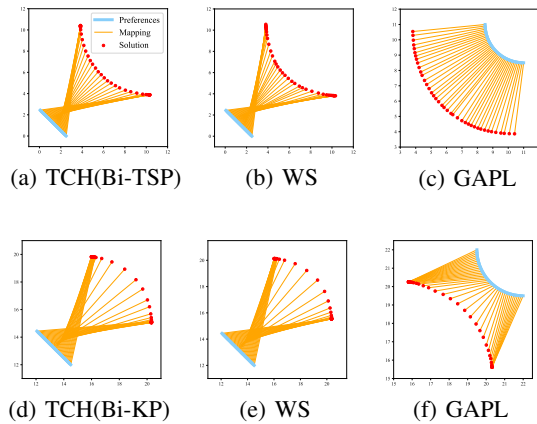


Figure 3: Visual comparisons on Bi-TSP20 and Bi-KP20. GAPL has better adaptability than WS- and TCH-based approaches.

This visualization supports our idea from three perspectives: 1) In terms of the true PF with uniformly distributed solutions (e.g. MOTSP), WS and TCH-based PMOCO tend to produce a large number of duplicate solutions at the corner of PF. In contrast, GAPL demonstrates a better understanding of the PF’s characteristics by avoiding duplicate solutions. 2) When examining the true PF with non-uniformly distributed solutions (e.g., MOKP), WS- and TCH-based methods struggle to find solutions in sparse regions, while GAPL effectively simulates the nonuniform distribution characteristics and successfully locates solutions in such areas. 3) The mappings generated by GAPL exhibit distinct geometric representations that are not achievable by other decomposition-based approaches. These observations lead us to conclude that GAPL demonstrates exceptional adaptability due to its geometric awareness. More visualization results are presented in Appendix M.4.

## 6 Conclusion

This paper proposes a GAPL for MOCO, offering a novel geometric perspective and addressing several drawbacks of previous decomposition-based methods. HRU strategy makes the Pareto attention model better utilize the local and non-local information of the PS/PF. Furthermore, the  $EI^2$  approach provides high-quality solutions with efficient approximate HV while LSSA enhances selection effi-

ciency. Experimental results on three well-known MOCO problems demonstrate the superiority of GAPL, particularly in terms of superior decomposition and efficient diversity enhancement. It should be noted that, like other neural heuristics, GAPL does not guarantee obtaining the exact PF. For future work, we plan to extend GAPL to other constrained MOCO problems and real-world applications.

## References

- [1] Matthias Ehrgott and Xavier Gandibleux. A survey and annotated bibliography of multiobjective combinatorial optimization. *OR-spektrum*, 22:425–460, 2000.
- [2] Zesong Fei, Bin Li, Shaoshi Yang, Chengwen Xing, Hongbin Chen, and Lajos Hanzo. A survey of multi-objective optimization in wireless sensor networks: Metrics, algorithms, and open problems. *IEEE Communications Surveys & Tutorials*, 19(1):550–586, 2016.
- [3] Sandra Zajac and Sandra Huber. Objectives and methods in multi-objective routing problems: a survey and classification scheme. *European journal of operational research*, 290(1):1–25, 2021.
- [4] Po-Lung Yu. Cone convexity, cone extreme points, and nondominated solutions in decision problems with multiobjectives. *Journal of optimization Theory and Applications*, 14:319–377, 1974.
- [5] Matthias Ehrgott, Xavier Gandibleux, and Anthony Przybylski. Exact methods for multi-objective combinatorial optimisation. *Multiple criteria decision analysis: State of the art surveys*, pages 817–850, 2016.
- [6] Arne Herzel, Stefan Ruzika, and Clemens Thielen. Approximation methods for multiobjective optimization problems: A survey. *INFORMS Journal on Computing*, 33(4):1284–1299, 2021.
- [7] Kaiwen Li, Tao Zhang, and Rui Wang. Deep reinforcement learning for multiobjective optimization. *IEEE transactions on cybernetics*, 51(6):3103–3114, 2020.
- [8] Xi Lin, Zhiyuan Yang, and Qingfu Zhang. Pareto set learning for neural multi-objective combinatorial optimization. *arXiv preprint arXiv:2203.15386*, 2022.
- [9] Qingfu Zhang and Hui Li. Moea/d: A multiobjective evolutionary algorithm based on decomposition. *IEEE Transactions on evolutionary computation*, 11(6):712–731, 2007.
- [10] Jinbiao Chen, Zizhen Zhang, Zhiguang Cao, Yaoxin Wu, Yining Ma, Te Ye, and Jiahai Wang. Neural multi-objective combinatorial optimization with diversity enhancement. *arXiv preprint arXiv:2310.15195*, 2023.
- [11] Tobias Friedrich, Christian Horoba, and Frank Neumann. Multiplicative approximations and the hypervolume indicator. In *Proceedings of the 11th Annual conference on Genetic and evolutionary computation*, pages 571–578, 2009.
- [12] Jingda Deng and Qingfu Zhang. Approximating hypervolume and hypervolume contributions using polar coordinate. *IEEE Transactions on Evolutionary Computation*, 23(5):913–918, 2019.
- [13] Richard Zhang and Daniel Golovin. Random hypervolume scalarizations for provable multi-objective black box optimization. In *International Conference on Machine Learning*, pages 11096–11105. PMLR, 2020.
- [14] Xiaoyuan Zhang, Xi Lin, Bo Xue, Yifan Chen, and Qingfu Zhang. Hypervolume maximization: A geometric view of pareto set learning. In *Thirty-seventh Conference on Neural Information Processing Systems*, 2023.
- [15] Kostas Florios and George Mavrotas. Generation of the exact pareto set in multi-objective traveling salesman and set covering problems. *Applied Mathematics and Computation*, 237: 1–19, 2014.
- [16] Kalyanmoy Deb, Amrit Pratap, Sameer Agarwal, and TAMT Meyarivan. A fast and elitist multiobjective genetic algorithm: Nsga-ii. *IEEE transactions on evolutionary computation*, 6(2):182–197, 2002.

- [17] Jialong Shi, Jianyong Sun, Qingfu Zhang, Haotian Zhang, and Ye Fan. Improving pareto local search using cooperative parallelism strategies for multiobjective combinatorial optimization. *IEEE Transactions on Cybernetics*, 2022.
- [18] Irwan Bello, Hieu Pham, Quoc V Le, Mohammad Norouzi, and Samy Bengio. Neural combinatorial optimization with reinforcement learning. *arXiv preprint arXiv:1611.09940*, 2016.
- [19] Mohammadreza Nazari, Afshin Oroojlooy, Lawrence Snyder, and Martin Takác. Reinforcement learning for solving the vehicle routing problem. *Advances in neural information processing systems*, 31, 2018.
- [20] Oriol Vinyals, Meire Fortunato, and Navdeep Jaitly. Pointer networks. *Advances in neural information processing systems*, 28, 2015.
- [21] Wouter Kool, Herke Van Hoof, and Max Welling. Attention, learn to solve routing problems! *arXiv preprint arXiv:1803.08475*, 2018.
- [22] Yeong-Dae Kwon, Jinho Choo, Byoungjip Kim, Iljoo Yoon, Youngjune Gwon, and Seungjai Min. Pomo: Policy optimization with multiple optima for reinforcement learning. *Advances in Neural Information Processing Systems*, 33:21188–21198, 2020.
- [23] Yining Ma, Jingwen Li, Zhiguang Cao, Wen Song, Le Zhang, Zhenghua Chen, and Jing Tang. Learning to iteratively solve routing problems with dual-aspect collaborative transformer. *Advances in Neural Information Processing Systems*, 34:11096–11107, 2021.
- [24] Hao Lu, Xingwen Zhang, and Shuang Yang. A learning-based iterative method for solving vehicle routing problems. In *International conference on learning representations*, 2019.
- [25] Aviv Navon, Aviv Shamsian, Gal Chechik, and Ethan Fetaya. Learning the pareto front with hypernetworks. *arXiv preprint arXiv:2010.04104*, 2020.
- [26] Xi Lin, Hui-Ling Zhen, Zhenhua Li, Qing-Fu Zhang, and Sam Kwong. Pareto multi-task learning. *Advances in neural information processing systems*, 32, 2019.
- [27] Yongxin Zhang, Jiahai Wang, Zizhen Zhang, and Yalan Zhou. Modrl/d-el: multiobjective deep reinforcement learning with evolutionary learning for multiobjective optimization. In *2021 International Joint Conference on Neural Networks (IJCNN)*, pages 1–8. IEEE, 2021.
- [28] Zizhen Zhang, Zhiyuan Wu, Hang Zhang, and Jiahai Wang. Meta-learning-based deep reinforcement learning for multiobjective optimization problems. *IEEE Transactions on Neural Networks and Learning Systems*, 2022.
- [29] Jinbiao Chen, Jiahai Wang, Zizhen Zhang, Zhiguang Cao, Te Ye, and Siyuan Chen. Efficient meta neural heuristic for multi-objective combinatorial optimization. *arXiv preprint arXiv:2310.15196*, 2023.
- [30] Michael Emmerich, Nicola Beume, and Boris Naujoks. An emo algorithm using the hypervolume measure as selection criterion. In *International Conference on Evolutionary Multi-Criterion Optimization*, pages 62–76. Springer, 2005.
- [31] Eckart Zitzler, Dimo Brockhoff, and Lothar Thiele. The hypervolume indicator revisited: On the design of pareto-compliant indicators via weighted integration. In *Evolutionary Multi-Criterion Optimization: 4th International Conference, EMO 2007, Matsushima, Japan, March 5-8, 2007. Proceedings 4*, pages 862–876. Springer, 2007.
- [32] Timo M Deist, Monika Grewal, Frank JWM Dankers, Tanja Alderliesten, and Peter AN Bosman. Multi-objective learning using hv maximization. In *International Conference on Evolutionary Multi-Criterion Optimization*, pages 103–117. Springer, 2023.
- [33] Ke Shang, Hisao Ishibuchi, Min-Ling Zhang, and Yiping Liu. A new r2 indicator for better hypervolume approximation. In *Proceedings of the Genetic and Evolutionary Computation Conference*, pages 745–752, 2018.

- [34] Eckart Zitzler and Lothar Thiele. Multiobjective evolutionary algorithms: a comparative case study and the strength pareto approach. *IEEE transactions on Evolutionary Computation*, 3(4): 257–271, 1999.
- [35] Claus Hillermeier. *Nonlinear multiobjective optimization: a generalized homotopy approach*, volume 135. Springer Science & Business Media, 2001.
- [36] Jürgen Schmidhuber. Learning to control fast-weight memories: An alternative to dynamic recurrent networks. *Neural Computation*, 4(1):131–139, 1992.
- [37] Aviv Shamsian, Aviv Navon, Ethan Fetaya, and Gal Chechik. Personalized federated learning using hypernetworks. In *International Conference on Machine Learning*, pages 9489–9502. PMLR, 2021.
- [38] Elad Sarafian, Shai Keynan, and Sarit Kraus. Recomposing the reinforcement learning building blocks with hypernetworks. In *International Conference on Machine Learning*, pages 9301–9312. PMLR, 2021.
- [39] Wei Ying, Yu Zhang, Junzhou Huang, and Qiang Yang. Transfer learning via learning to transfer. In *International Conference on Machine Learning*, pages 5085–5094. PMLR, 2018.
- [40] Zihan Wang, Bochao Mao, Hao Hao, Wenjing Hong, Chunyun Xiao, and Aimin Zhou. Enhancing diversity by local subset selection in evolutionary multiobjective optimization. *IEEE Transactions on Evolutionary Computation*, 2022.
- [41] Thibaut Lust and Jacques Teghem. The multiobjective traveling salesman problem: a survey and a new approach. In *Advances in Multi-Objective Nature Inspired Computing*, pages 119–141. Springer, 2010.
- [42] Philippe Lacomme, Christian Prins, and Marc Sevaux. A genetic algorithm for a bi-objective capacitated arc routing problem. *Computers & Operations Research*, 33(12):3473–3493, 2006.
- [43] Cristina Bazgan, Hadrien Hugot, and Daniel Vanderpooten. Solving efficiently the 0–1 multi-objective knapsack problem. *Computers & Operations Research*, 36(1):260–279, 2009.
- [44] Renato Tinós, Keld Helsgaun, and Darrell Whitley. Efficient recombination in the lin-kernighan-helsgaun traveling salesman heuristic. In *Parallel Problem Solving from Nature–PPSN XV: 15th International Conference, Coimbra, Portugal, September 8–12, 2018, Proceedings, Part I 15*, pages 95–107. Springer, 2018.
- [45] Charles Audet, Jean Bigeon, Dominique Cartier, Sébastien Le Digabel, and Ludovic Salomon. Performance indicators in multiobjective optimization. *European journal of operational research*, 292(2):397–422, 2021.
- [46] Kaisa Miettinen. *Nonlinear multiobjective optimization*, volume 12. Springer Science & Business Media, 1999.
- [47] Doug P Hardin, Edward B Saff, et al. Discretizing manifolds via minimum energy points. *Notices of the AMS*, 51(10):1186–1194, 2004.
- [48] Sergiy V Borodachov, Douglas P Hardin, and Edward B Saff. *Discrete energy on rectifiable sets*. Springer, 2019.
- [49] Jesús Guillermo Falcón-Cardona, Hisao Ishibuchi, and Carlos A Coello Coello. Exploiting the trade-off between convergence and diversity indicators. In *2020 IEEE Symposium Series on Computational Intelligence (SSCI)*, pages 141–148. IEEE, 2020.
- [50] Raquel Hernández Gómez and Carlos A Coello Coello. A hyper-heuristic of scalarizing functions. In *Proceedings of the genetic and evolutionary computation conference*, pages 577–584, 2017.
- [51] Julian Blank, Kalyanmoy Deb, Yashesh Dhebar, Sunith Bandaru, and Haitham Seada. Generating well-spaced points on a unit simplex for evolutionary many-objective optimization. *IEEE Transactions on Evolutionary Computation*, 25(1):48–60, 2020.
- [52] Kurt Hornik, Maxwell Stinchcombe, and Halbert White. Multilayer feedforward networks are universal approximators. *Neural networks*, 2(5):359–366, 1989.

## A Limitations

The main limitation of GAPL is that the design of our reward function is designed by empirical results. In our experiment, we find that both local and non-local term present different influence in different stages of training. To be specific, the non-local term is difficult to study compared with local term while the non-local term contains more information. Therefore, we introduce two adaptive parameters to control the ratio of them according to the state of training. In the future, we will further study the connection between them to design more suitable reward function with theoretically sound.

## B Broader Impact

In our paper, we propose Geometry-Aware Pareto set Learning algorithm, The positive impact can be analyzed from two aspects. To begin with, we design a novel reward function, which includes local term and non-local term. It is the first time to introduce global information in the reward function. Therefore, the mapping from preferences to objective space in GAPL is clearer than the previous methods. Secondly, the introduction of approximate HV can speed up the neural network to extract global information, which has reference significance for the follow-up methods. Lastly, we design a novel inference method compared with previous simple methods.

On the negative side, the reward function without theoretical guarantee shows remarkable improvement in most benchmark problems. However, the performance on real-world engineering design needs to be further tested to ensure safety.

## C Hardware Settings

All the experiments are conducted with an RTX 4090 GPU and a 1.5GHz AMD EPYC 7742 CPU.

## D Aggregation Function

An aggregated (or utility) function can map each point in the objective space into a scalar according to an  $m$ -dimensional weight vector  $\lambda$  with  $\|\lambda\|_p = 1$  ( $l_p$ -norm constraint) and  $\lambda_i \geq 0$ . Weighted-Sum (WS) and Weighted-Tchebycheff are commonly used utility functions [46]. As the simplest representative, WS can be defined by  $\min_{\mathbf{x} \in \mathcal{X}} f(\mathbf{x}|\lambda) = \sum_{i=1}^M \lambda_i f_i(\mathbf{x})$ .

## E Reference Points and Ideal Points

For a problem, all methods share the same reference point  $\mathbf{r}$  and ideal point  $\mathbf{z}$ , as shown in Table 3.

## F Extension of Lemma 4.1 to Infinite Set

Lemma 4.1 with a finite number of objective vectors can be extended to an infinite set, which can also be expressed as an expectation [14]:

$$\mathcal{H}\mathcal{V}_r(Y) = \frac{\Phi}{m2^m} \mathbb{E}_\theta[(\mathcal{V}_\mathcal{X}(\theta))^m], \quad (8)$$

where  $\mathcal{V}_\mathcal{X}(\theta)$  denotes the Euclidean distance between the reference point and the PF with the polar angle  $\theta$  (see Figure 4). Moreover,  $\mathcal{V}_\mathcal{X}(\theta)$  can be precisely evaluated using the following equation:

$$\mathcal{V}_\mathcal{X}(\theta) = \max_{\mathbf{x} \in \mathcal{X}} \mathcal{G}^{mtch}(f(\mathbf{x}), \theta) = \max_{\mathbf{x} \in \mathcal{X}} \min_{i \in \{1, \dots, m\}} \{(r_i - f_i(x_i)) / \lambda_i(\theta)\}, \quad (9)$$

where  $\mathcal{G}^{mtch}(f(\mathbf{x}), \theta)$  represents the projected distance of an objective vector  $f(\mathbf{x})$  with polar angle  $\theta$  (see Figure 4). Moreover, the optimal solution  $\mathbf{x}$  of  $\mathcal{V}_\mathcal{X}(\theta)$  has the following properties: 1) satisfies  $\frac{r_1 - y_1(\mathbf{x})}{\lambda_1(\theta)} = \dots = \frac{r_m - f_m(\mathbf{x})}{\lambda_m(\theta)}$ ; 2) is Pareto optimal. Directly optimizing  $\mathcal{H}\mathcal{V}_r$  in Eq. 2 is challenging (time-consuming). However, [14] provides an easy-to-compute form of the HV, denoted by  $\widetilde{HV}_r(\beta)$ :

$$\begin{aligned} \widetilde{HV}_r(\beta, \theta^{P'}, s) &= \frac{\Phi}{m2^m} \mathbb{E}_{\theta^{P'}}[(\mathcal{V}_\beta(\theta^i, s))^m], \\ \mathcal{V}_\beta(\theta, s) &= \max(\mathcal{G}^{mtch}(f(\Psi_\beta(\theta, s)), \theta), 0) \end{aligned} \quad (10)$$

Table 3: Description of synthetic benchmarks we used in this work.

Problem	Size	reference point ( $\mathbf{r}$ )	ideal point ( $\mathbf{z}$ )
Bi-TSP	20	(20, 20)	(0, 0)
	50	(35, 35)	(0, 0)
	100	(65, 65)	(0, 0)
Bi-CVRP	20	(15, 3)	(0, 0)
	50	(40, 3)	(0, 0)
	100	(60, 3)	(0, 0)
Bi-KP	50	(5, 5)	(30, 30)
	100	(20, 20)	(50, 50)
	200	(30, 30)	(75, 75)
Tri-TSP	20	(20, 20, 20)	(0, 0, 0)
	50	(35, 35, 35)	(0, 0, 0)
	100	(65, 65, 65)	(0, 0, 0)

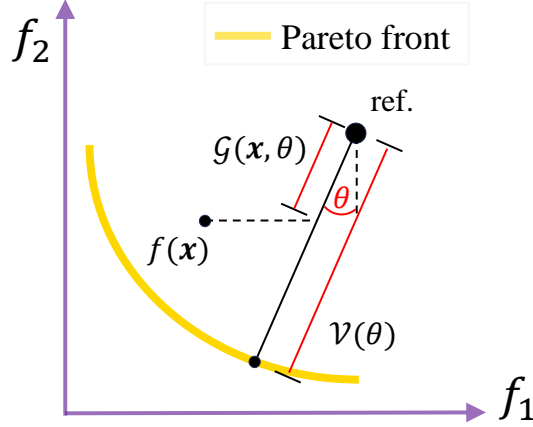


Figure 4: Pareto front hypervolume calculation in the polar coordinate.  $\mathcal{G}(\mathbf{x}, \theta)$  is the distance from the reference point to the Pareto front along angle  $\theta$ .  $\mathcal{V}(\theta)$  is the projected distance at angle  $\theta$ .

where  $\theta^{P'} = \{\theta^1, \dots, \theta^{P'}\}$  denotes the polar angles for all the subproblems in the polar angles pool,  $\mathcal{V}_\beta(\theta, s)$  is the projected distance in Eq. 9 ( $0 \leq \mathcal{V}_\beta(\theta, s) \leq \mathcal{V}_\mathcal{X}(\theta)$ ) if there is an optimal solution in  $\mathcal{X}$ . When the Pareto attention model is well-trained,  $\mathcal{V}_\beta(\theta, s) \rightarrow \mathcal{V}_\mathcal{X}(\theta)$ ,  $\forall \theta \in \text{Unif}(\Theta)$  and thus  $\widetilde{\mathcal{H}\mathcal{V}_r(\beta)} \rightarrow \mathcal{H}\mathcal{V}_r(Y)$ .

## G Details of Local Subset Selection Acceleration

### G.1 Local Subset Selection

For an optimization problem  $S^* = \arg \min_{S \in \Omega} f(S)$ , where  $S$  denotes a subset,  $\Omega$  denotes the search space and  $f(\cdot)$  denotes quantization function of subset quality, a general procedure of a local selection algorithm can be summarized as follows:

1. Select an initial subset  $S$ ;
2. Define the neighborhood  $\mathcal{N}(S) \subset \Omega$ ;
3. Move to a neighbor  $S \leftarrow S' \in \mathcal{N}(S)$  if  $f(S') < f(S)$ ;
4. Go to step 2 if the termination condition is not met; otherwise, output  $S$ .

**Definition G.1 (Neighborhood)** In our case, a solution  $S$  in a local selection is actually a set that contains  $\mu$  solutions of the multi-objective problems, the search space  $\Omega = \{S | S \subset Q, |S| = \mu\}$  contains all the subsets of the given population  $Q$  with size  $\mu$ . It is clear that  $|\Omega| = C_{\mu+\lambda}^{\mu}$ . Define the distance between  $S$  and  $S'$  as the size of their symmetric difference:

$$dis(S, S') = |\{x | x \in S, x \notin S'\} \cup \{x \in S', x \notin S\}|. \quad (11)$$

Then, the neighborhood of  $S$  can be defined as follows:

$$\mathcal{N}(S) = \{S' | dis(S, S') \leq \epsilon, S' \in \Omega\}, \quad (12)$$

where  $\epsilon$  is a threshold that defines the range of the neighborhood of  $S$ . It is clear that the minimum value of  $\epsilon$  is 2, and in such case the size of the neighborhood is  $|\mathcal{N}(S)| = \mu \times \lambda$ . In this article, we only consider the situation when  $\epsilon = 2$ . In such case, the neighborhood can be also formulated as follows:

$$\mathcal{N}(S) = \{S \setminus \{x\} \cup \{x'\} | x \in S, x' \in P \setminus S\}. \quad (13)$$

In implementation, we can enumerate all the neighbor solutions of  $S$  by replacing an element with another one from the set  $Q \setminus S$ .

---

**Algorithm 2: Local Subset Selection**

---

**input** : the given population  $Q_1$ , quantization function of subset quality  $f$   
**output** : the optimal subset  $Q^*$

- 1 Generate an initial subset  $Q^* \subset Q_1$
- 2 Set  $Q_2 = Q_1 \setminus Q^*$
- 3 **while True do**
- 4 Set  $x, y = \arg \min_{x \in Q^*, y \in Q_2} f(Q^* \setminus \{x\} \cup \{y\})$
- 5 **if**  $f(Q^* \setminus \{x\} \cup \{y\}) < f(Q^*)$  **then**
- 6  $Q^* = Q^* \setminus \{x\} \cup \{y\}$
- 7  $Q_2 = Q_2 \setminus \{y\} \cup \{x\}$
- 8 **else**
- 9 Output  $Q^*$  and stop
- 10 **end**
- 11 **end**

---

Algorithm 2 presents the proposed subset selection based on a local search. In line 2, the initial subset is generated by using the parent solutions; in line 5, the best neighbor of  $P^*$  is found by enumerating all of its neighbors; in lines 6–8, the subset moves to its neighbor if a better one is found; the algorithm terminates in line 10 when no better neighbor could be found, and a local optimal subset is guaranteed.

## G.2 Advantages of Potential Energy Function

The potential energy model has been widely used in discretizing manifolds [47, 48], Recently, several traditional optimization researchers tried to adopt similar ideas to improve the diversity of solutions [49, 50] and/or to generate well-distributed reference points [51], since it has the following properties.

1. **High Sensitivity:** It is highly sensitive to data distribution. A local unevenness of solutions will intensely contribute to the overall metric value, so it could provide strong guidance for the spacing of solutions, providing high selection pressure;
2. **Low Computing Complexity:** Compared with the HV metric, the potential energy of a system is easy to calculate. An accurate value can be calculated with a time complexity of  $O(n_1^2 m)$ . Besides, it satisfies the following additional rule, which favors the calculation:

$$\begin{cases} E_{x \notin Q}(Q \cup \{x\}) = E(Q) + 2 \sum_{y \in Q} U(y, x) \\ E_{x \in Q}(Q \setminus \{x\}) = E(Q) - 2 \sum_{y \in Q, y \neq x} U(y, x) \end{cases} \quad (14)$$

3. Geometric Insensitive: The minimal energy configuration is shape-insensitive, which means uniformly distributed solutions can be obtained regardless of the shape of the optimal PF by minimizing the potential energy.

For these reasons, our algorithm uses the potential energy function as the subset selection objective, i.e.,  $f(S) = E(S)$ . Moreover, We recommend using  $c = 2m$  in this article via ablation study.

### G.3 Proofs of Eq. 7 and the Difference of Contributions Between Solutions

$Q_1$  contains currently selected solutions and  $Q_2$  contains the unselected ones. Then, the contribution of a selected one  $e1(\mathbf{x})$  and an unselected one  $e2(\mathbf{x})$  according to the systems  $Q_1$  can be defined as follows:

$$\begin{cases} e1(\mathbf{x}) = \sum_{\mathbf{y} \in Q_1 \setminus \mathbf{x}} U(\mathbf{x}, \mathbf{y}) \\ e2(\mathbf{x}) = \sum_{\mathbf{y} \in Q_1} U(\mathbf{x}, \mathbf{y}) \end{cases} \quad (15)$$

Thus, induced from Eq. 6 and Eq. 15, the following equality always holds:

$$E(P \setminus \{\mathbf{x}\} \cup \{\mathbf{y}\}) = E(P) - e1(\mathbf{x}) + e2(\mathbf{y}) - U(\mathbf{x}, \mathbf{y}). \quad (16)$$

Consider one of  $Q_1$ 's neighbors  $Q_1 \setminus \{\mathbf{x}\} \cup \{\mathbf{y}\}$ , where  $\mathbf{x} \in Q_1$  and  $\mathbf{y} \in Q_2$ . We can have the following proof for the difference between the energy of  $Q_1$  and  $Q_1 \setminus \{\mathbf{x}\} \cup \{\mathbf{y}\}$ :

$$\begin{aligned} \Delta E(Q_1) &= E(Q_1) - E(Q_1 \setminus \{\mathbf{x}\} \cup \{\mathbf{y}\}) \\ &= E(Q_1) - \sum_{\mathbf{x}' \in Q_1 \setminus \{\mathbf{x}\} \cup \{\mathbf{y}\}} \sum_{\mathbf{x}'' \in Q_1 \setminus \{\mathbf{x}, \mathbf{x}'\} \cup \{\mathbf{y}\}} U(\mathbf{x}', \mathbf{x}'') \\ &= E(Q_1) - \left( \sum_{\mathbf{x}' \in Q_1} \sum_{\mathbf{x}'' \in Q_1 \setminus \{\mathbf{x}'\}} U(\mathbf{x}', \mathbf{x}'') - \sum_{\mathbf{x}' \in Q_1 \setminus \{\mathbf{x}\}} U(\mathbf{x}, \mathbf{x}') + \sum_{\mathbf{x}' \in Q_1} U(\mathbf{y}, \mathbf{x}') - U(\mathbf{x}, \mathbf{y}) \right) \\ &= E(Q_1) - (E(Q_1) - e1(\mathbf{x}) + e2(\mathbf{y}) - U(\mathbf{x}, \mathbf{y})) \\ &= e1(\mathbf{x}) - e2(\mathbf{y}) + U(\mathbf{x}, \mathbf{y}). \end{aligned} \quad (17)$$

It is clear that when evaluating the neighbor of  $Q_1$  by replacing  $\mathbf{x}$  by  $\mathbf{y}$ , it is not necessary to calculate the energy of the new system. Instead, only the difference between the energy values of the two systems is needed, i.e. Eq. 7.  $\square$

Similarly, we can calculate the difference between the contributions of selected and unselected solutions.

Considering a solution  $\mathbf{x}' \in Q_1$ , if  $\mathbf{x}' \neq \mathbf{x}$ , we can have following proof:

$$\begin{aligned} \Delta e1(\mathbf{x}') &= \sum_{\mathbf{x}'' \in Q_1 \setminus \{\mathbf{x}'\}} U(\mathbf{x}', \mathbf{x}'') - \sum_{\mathbf{x}'' \in Q_1 \setminus \{\mathbf{x}', \mathbf{x}\} \cup \{\mathbf{y}\}} U(\mathbf{x}', \mathbf{x}'') \\ &= \left( \sum_{\mathbf{x}'' \in Q_1 \setminus \{\mathbf{x}', \mathbf{x}\}} U(\mathbf{x}', \mathbf{x}'') + U(\mathbf{x}', \mathbf{x}) \right) - \left( \sum_{\mathbf{x}'' \in Q_1 \setminus \{\mathbf{x}', \mathbf{x}\}} U(\mathbf{x}', \mathbf{x}'') + U(\mathbf{x}', \mathbf{y}) \right) \\ &= U(\mathbf{x}', \mathbf{x}) - U(\mathbf{x}', \mathbf{y}). \end{aligned} \quad (18)$$

If  $\mathbf{x}' = \mathbf{x}$ :

$$\begin{aligned} \Delta e1(\mathbf{x}') &= \sum_{\mathbf{x}'' \in Q_1 \setminus \{\mathbf{x}'\}} U(\mathbf{x}', \mathbf{x}'') - \sum_{\mathbf{x}'' \in Q_1 \setminus \{\mathbf{x}'\} \cup \{\mathbf{y}\}} U(\mathbf{x}', \mathbf{x}'') \\ &= \sum_{\mathbf{x}'' \in Q_1 \setminus \{\mathbf{x}'\}} U(\mathbf{x}', \mathbf{x}'') - \left( \sum_{\mathbf{x}'' \in Q_1 \setminus \{\mathbf{x}'\}} U(\mathbf{x}', \mathbf{x}'') + U(\mathbf{x}', \mathbf{y}) \right) \\ &= -U(\mathbf{x}', \mathbf{y}). \end{aligned} \quad (19)$$



Considering a solution  $\mathbf{y}' \in Q_2$ , if  $\mathbf{y}' \neq \mathbf{y}$ , we can have following proof:

$$\begin{aligned}
\Delta e2(\mathbf{y}') &= \sum_{\mathbf{x}'' \in Q_1} U(\mathbf{y}', \mathbf{x}'') - \sum_{\mathbf{x}'' \in Q_1 \setminus \{\mathbf{x}\} \cup \{\mathbf{y}\}} U(\mathbf{y}', \mathbf{x}'') \\
&= \sum_{\mathbf{x}'' \in Q_1} U(\mathbf{y}', \mathbf{x}'') - \left( \sum_{\mathbf{x}'' \in Q_1} U(\mathbf{y}', \mathbf{x}'') - U(\mathbf{y}', \mathbf{x}) + U(\mathbf{y}', \mathbf{y}) \right) \\
&= U(\mathbf{y}', \mathbf{x}) - U(\mathbf{y}', \mathbf{y}).
\end{aligned} \tag{20}$$

If  $\mathbf{y}' = \mathbf{y}$ :

$$\begin{aligned}
\Delta e2(\mathbf{y}') &= \sum_{\mathbf{x}'' \in Q_1} U(\mathbf{y}', \mathbf{x}'') - \sum_{\mathbf{x}'' \in Q_1 \setminus \{\mathbf{x}\}} U(\mathbf{y}', \mathbf{x}'') \\
&= \sum_{\mathbf{x}'' \in Q_1} U(\mathbf{y}', \mathbf{x}'') - \left( \sum_{\mathbf{x}'' \in Q_1} U(\mathbf{y}', \mathbf{x}'') - U(\mathbf{y}', \mathbf{x}) \right) \\
&= U(\mathbf{y}', \mathbf{x}).
\end{aligned} \tag{21}$$

In summary:

$$\begin{aligned}
\Delta e1(\mathbf{x}') &= \begin{cases} U(\mathbf{x}', \mathbf{x}) - U(\mathbf{x}', \mathbf{y}), & \mathbf{x}' \in Q_1 \setminus \{\mathbf{x}\} \\ -U(\mathbf{x}', \mathbf{y}), & \mathbf{x}' = \mathbf{x} \end{cases} \\
\Delta e2(\mathbf{y}') &= \begin{cases} U(\mathbf{y}', \mathbf{x}) - U(\mathbf{y}', \mathbf{y}), & \mathbf{y}' \in Q_2 \setminus \{\mathbf{y}\} \\ U(\mathbf{y}', \mathbf{x}), & \mathbf{y}' = \mathbf{y} \end{cases}.
\end{aligned} \tag{22}$$

□

## H Model Architecture

The core architecture of the base model is similar with POMO, composed of an encoder and a decoder. For node features  $\mathbf{x}_1, \dots, \mathbf{x}_n$  and previous solutions  $\mathcal{F}$ , the encoder first computes initial node embeddings  $\mathbf{g}_1^{(0)}, \dots, \mathbf{g}_n^{(0)} \in \mathcal{R}^d (d = 128)$  and previous solution information by a linear projection. The final node embeddings  $\mathbf{g}_1^{(L)}, \dots, \mathbf{g}_n^{(L)}$  are further computed by  $L = 6$  attention layers. Each attention layer is composed of a multi-head attention (MHA) with  $M = 8$  heads and fully connected feed-forward sublayer. Each sublayer adds a skip-connection and batch normalization, as follows:

$$\mathbf{g}_i^{(l)} = \text{BN}(\hat{\mathbf{g}}_i + \text{FF}(\hat{\mathbf{g}}_i)). \tag{23}$$

The decoder sequentially chooses a node according to a probability distribution produced by the node embeddings to construct a solution. The total decoding step  $T$  is determined by the specific problem. The HV network is employed to tackle the preference  $\theta$  for the corresponding subproblem. Specifically, according to the given  $\theta$ , the HV network generates the decoder parameters of the MHA model  $\beta$ , which is an encoder-decoder-styled architecture, i.e.,  $\beta(\theta, s) = [\beta_{en}(s), \beta_{de}(\boldsymbol{\pi})]$ . The HV network adopts a simple MLP model with two 256-dimensional hidden layers and ReLU activation. The MLP first maps an input with  $M + 2$  dimensions to a hidden embedding  $g(\theta)$ , which is then used to generate the decoder parameters by linear projection. At step  $t$  in the decoding procedure, the glimpse  $\mathbf{q}_c$  of the context embedding  $\mathbf{h}_c$  is computed by the MHA layer. Then, the compatibility  $u$  is calculated as follows,

$$u_i = \begin{cases} -\infty, & \text{node } i \text{ is masked} \\ C \cdot \tanh\left(\frac{\mathbf{q}_c^T (W^K \mathbf{g}_i^{(L)})}{\sqrt{d/Y}}\right), & \text{otherwise} \end{cases}. \tag{24}$$

where  $C$  is set to 10 [21]. Finally, softmax is employed to calculate the selection probability distribution  $\text{Prob}_\beta(\boldsymbol{\pi} | s, \theta^i, \mathcal{F}_i^j)$  for nodes, i.e.,  $\text{Prob}_\beta(\pi_t | \boldsymbol{\pi}_{1:t-1}, s, \theta^i, \mathcal{F}_i^j) = \text{Softmax}(u)$ .

---

**Algorithm 3:** The inference process of GAPL

---

**input** : preference distribution  $\Theta$ , instance distribution  $\mathcal{S}$ , number of uniformly distributed preferences (polar angles)  $P$ , batch size  $B$ , instance size  $N$ , model parameter  $\beta$   
**output** : The final solution set  $\mathbf{Y}$

- 1  $Pref \leftarrow P$  uniformly distributed preferences are generated according to  $\Theta$ .
- 2  $s_i \sim \mathbf{SampleInstance}(\mathcal{S}) \quad \forall i \in \{1, \dots, B\}$
- 3 Initialize  $\mathcal{F}_i^j \leftarrow \emptyset \quad \forall i, j \in \{1, \dots, N\}$
- 4 Initialize  $\theta^0 \leftarrow \emptyset$
- 5 Initialize  $\mathbf{Y} \leftarrow \emptyset$
- 6 **for**  $p = 1$  **to**  $P$  **do**
- 7      $\theta^p \leftarrow \theta^{p-1} \cup Pref_p$
- 8      $\pi_i^j \sim \mathbf{SampleSolution}$
- 9      $(Prob_{\beta(\theta)}(\cdot | s_i, \theta), \mathcal{F}_i^j) \mathcal{V}_{\beta}(\theta, s), \widetilde{\mathcal{H}}\mathcal{V}_r(\beta, \theta^p, s) \leftarrow$  Calculate the projection distance and approximate HV by Eq. 10  $\forall i, j$
- 10      $\alpha_i^j \leftarrow$  Calculate expected HV improvement by Eq. 5  $\quad \forall i, j$
- 11      $R_{i,1}^j \leftarrow$  Calculate the reward only by the local term of Eq. 4  $\quad \forall i, j$  //Explicit inference
- 12      $R_{i,2}^j \leftarrow$  Calculate the reward by both the local and the non-local term of Eq. 4 according to parameter  $\alpha_i^j \quad \forall i, j$  //Implicit inference
- 13      $\pi_{i,1}, \pi_{i,2} \leftarrow \mathbf{Argmax}(R_{i,1}^j), \mathbf{Argmax}(R_{i,2}^j) \quad \forall j$
- 14      $\mathcal{F}_i^j \leftarrow \mathcal{F}_i^j \cup \{\mathbf{f}(\pi_{i,1}), \mathbf{f}(\pi_{i,2})\} \quad \forall i, j$
- 15      $\mathbf{Y} \leftarrow \mathbf{Y} \cup \{\frac{1}{B} \sum_{i=1}^B \mathbf{f}(\pi_{i,1}), \sum_{i=1}^B \mathbf{f}(\pi_{i,2})\} \quad \forall i$
- 16 **end**
- 17  $\mathbf{Y} \leftarrow \mathbf{LSSA}(\mathbf{Y})$

---

## I Node Features and Context Embedding

The input dimensions of the node features vary with different problems. The inputs of the  $m$ -objective TSP are  $T$  nodes with  $2m$ -dimensional features. The inputs of Bi-CVRP are  $T$  customer nodes with 3-dimensional features and a depot node with 2-dimensional features. The inputs of Bi-KP are  $T$  nodes with 3-dimensional features. At step  $t$  in the decoder, a context embedding  $\mathbf{h}_c$  is used to calculate the probability of node selection. For MOTSP,  $\mathbf{h}_c$  is defined as the concatenation of the graph embedding  $\bar{\mathbf{h}} = \sum_{i=1}^n \mathbf{h}_i / T$ , the embedding of the first node  $\mathbf{h}_{\pi_1}$ , and the embedding of the last node  $\mathbf{h}_{\pi_{t-1}}$ . For MOCVRP,  $\mathbf{h}_c$  is defined as the concatenation of the graph embedding  $\bar{\mathbf{h}}$ , the embedding of the last node  $\mathbf{h}_{\pi_{t-1}}$ , and the remaining vehicle capacity. For MOKP,  $\mathbf{h}_c$  is defined as the concatenation of the graph embedding  $\bar{\mathbf{h}}$  and the remaining knapsack capacity.

A masking mechanism is adopted in each decoding step to ensure the feasibility of solutions. For MOTSP, the visited nodes are masked. For MOCVRP (MOKP), besides the visited nodes, those with a demand (weight) larger than the remaining vehicle (knapsack) capacity are also masked.

## J Inference Process of GAPL

In terms of the inference process of GAPL, we have adopted explicit and implicit dual inference (line 11-12) in 3 to generate solutions and applied local subset selection acceleration strategy to select elite solutions.

## K Instance Augmentation

Instance augmentation exploits multiple efficient transformations for the original instance that share the same optimal solution. Then, all transformed problems are solved and the best solution among them are finally selected. According to POMO, a 2D coordinate  $(x, y)$  has eight different transformations,  $\{(x, y), (y, x), (x, 1 - y), (y, 1 - x), (1 - x, y), (1 - y, x), (1 - x, 1 - y), (1 -$

$y, 1 - x\}$ . An instance of Bi-CVRP has 8 transformations, and an instance of  $m$ -objective TSP has  $8^m$  transformations [8] due to the full transformation permutation of  $m$  groups of 2-dimensional coordinates,.

## L An Alternative Form of GAPL

We also provide an alternative surrogate hypervolume function, denoted as GAPL-alter. Figure 5 shows details. We first define region  $S$  as the set of points dominating the Pareto front.

$$S = \{q | \exists p \in \mathcal{T} : p \prec q \text{ and } q \succ p^{ideal}\}. \quad (25)$$

We use the notation  $\Lambda(\cdot)$  to represent the Lebesgue measure of a set. Geometrically, as illustrated in Figure 5, it can be observed that:

$$\Lambda(S) + \mathcal{H}\mathcal{V}_r(Y) = \prod_{i=1}^m (r_i - z_i). \quad (26)$$

The volume of  $S$  can be calculated in a polar coordinate as follows,

$$\Lambda(S) = \frac{\Phi}{m2^m} \int_{(0, \frac{\pi}{2})^{(m-1)}} \bar{\mathcal{V}}(\theta). \quad (27)$$

Thus, the Pareto hypervolume can be estimated as the volume difference between the regions dominating  $r$  and those that dominate the Pareto front. GAPL-alter maximizes the following objective,

$$\begin{aligned} \widetilde{\mathcal{H}\mathcal{V}}_r(\beta, \theta^P, s) &= \prod_{i=1}^m (r_i - z_i) - \frac{\Phi}{m2^m} \mathbb{E}_{\theta^P} [(\bar{\mathcal{V}}_\beta(\theta^i, s))^m], \\ \bar{\mathcal{V}}_\beta(\theta, s) &= \max(\bar{\mathcal{G}}^{mtch}(f(\Psi_\beta(\theta, s)), \theta), 0) \end{aligned} \quad (28)$$

where  $\bar{\mathcal{G}}^{mtch}(\cdot)$  is an alternative projected distance function:

$$\bar{\mathcal{G}}^{mtch}(f(\Psi_\beta(\theta, s)), \theta) = \max_{i \in \{1, \dots, m\}} \{(y_i - z_i) / \lambda_i(\theta)\}. \quad (29)$$

Although the Pareto neural model  $\Psi_\beta(\cdot)$  theoretically has the ability to represent the complete

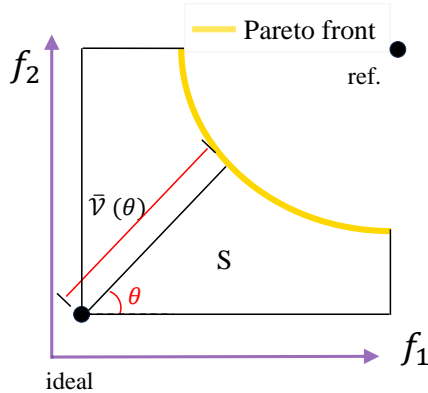


Figure 5: Alternative Pareto front hypervolume calculation in the polar coordinate.

Pareto set [52], empirical results show that the quality of the learned solutions is sensitive to the specific choice: Eq. 10 and Eq. 28 give different performances on various tasks. The main results of GAPL-alter can be found in Appendix M.1.

## M Additional experiments

### M.1 Main results of GAPL-alter and Analysis

As introduced in Appendix L, we provide an alternative form of GAPL, namely GAPL-alter. Figure 4 shows the results of GAPL-alter compared with several baselines. GAPL-alter also shows the best overall performance. Here, we want to discuss the nature of GAPL and GAPL-alter since they show different features on various problems. Specifically, GAPL-alter can show better performance on concave Pareto front (i.e. MOKP), while GAPL-alter can show better performance on non-concave Pareto front (i.e. MOTSP and MOCVRP). In terms of non-concave Pareto front, the projection distance  $\mathcal{V}_\beta(\theta)$  is uniformly distributed, which provides robustness for training model, while  $\mathcal{V}_\beta(\theta)$  is sensitive because of its non-uniform distribution which may lead to the overfitting of Pareto attention model. This phenomenon is the opposite on the question concave Pareto front. Therefore, it is necessary to choose different alternatives for specific problems.

Table 4: Experimental results on 200 random instances for MOCO problems.

Method	Bi-TSP20			Bi-TSP50			Bi-TSP100		
	HV $\uparrow$	Gap $\downarrow$	Time $\downarrow$	HV $\uparrow$	Gap $\downarrow$	Time $\downarrow$	HV $\uparrow$	Gap $\downarrow$	Time $\downarrow$
WS-LKH (101 pref.)	0.6268	0.70%	4.2m	0.6401	0.47%	41m	<b>0.7071</b>	<b>-0.06%</b>	2.6h
PPLS/D-C (200 iter.)	0.6256	0.89%	25m	0.6282	2.32%	2.7h	0.6845	3.14%	11h
NSGAIL-TSP	0.5941	5.88%	40m	0.5984	6.95%	43m	0.6643	6.00%	53m
DRL-MOA (101 models)	0.6257	0.87%	7s	0.6360	1.10%	10s	0.6971	1.36%	22s
PMOCO (101 pref.)	0.6266	0.73%	8s	0.6349	1.28%	13s	0.6953	1.61%	21s
NHDE-P (101 pref.)	0.6288	0.38%	4.3m	0.6389	0.65%	8.3m	0.7005	0.88%	16m
GAPL-alter (101 pref.)	<u>0.6301</u>	<u>0.17%</u>	18s	0.6394	0.58%	23s	0.7009	0.82%	31s
EMNH (aug.)	0.6271	0.65%	1.3m	0.6408	0.36%	4.6m	0.7023	0.62%	17m
PMOCO (101 pref. & aug.)	0.6273	0.62%	46s	0.6392	0.61%	3.1m	0.6997	0.99%	5.7m
NHDE-P (101 pref. & aug.)	0.6296	0.25%	9.8m	<u>0.6429</u>	<u>0.03%</u>	19m	0.7050	0.24%	40m
GAPL-alter (101 pref. & aug.)	<b>0.6312</b>	<b>0.00%</b>	1.2m	<b>0.6431</b>	<b>0.00%</b>	4.5m	<u>0.7067</u>	<u>0.00%</u>	6.8m
Method	Bi-CVRP20			Bi-CVRP50			Bi-CVRP100		
PPLS/D-C (200 iter.)	0.3351	3.98%	1.2h	0.4149	3.31%	9.6h	0.4083	1.80%	37h
NSGAIL-CVRP	0.3123	10.52%	37m	0.3631	15.38%	38m	0.3538	14.91%	43m
DRL-MOA (101 models)	0.3453	1.06%	7s	0.4270	0.49%	20s	<b>0.4176</b>	<b>-0.43%</b>	40s
PMOCO (101 pref.)	0.3467	0.66%	8s	0.4271	0.47%	18s	0.4131	0.65%	36s
NHDE-P (101 pref.)	0.3458	0.92%	1.5m	0.4248	1.00%	3.1m	0.4127	0.75%	5.3m
GAPL-alter (101 pref.)	0.3468	0.63%	17s	0.4272	0.44%	31s	0.4140	0.43%	58s
EMNH (aug.)	0.3471	0.54%	33s	0.4250	0.96%	1.4m	0.4146	0.29%	3.7m
PMOCO (101 pref. & aug.)	<u>0.3481</u>	<u>0.26%</u>	1m	0.4287	<u>0.09%</u>	2.1m	0.4150	0.19%	4.5m
NHDE-P (101 pref. & aug.)	0.3465	0.72%	5.1m	0.4262	0.68%	9.2m	0.4139	0.46%	21m
GAPL-alter (101 pref. & aug.)	<b>0.3490</b>	<b>0.00%</b>	2.2m	<b>0.4291</b>	<b>0.00%</b>	4.1m	<u>0.4158</u>	<u>0.00%</u>	6.8m
Method	Bi-KP50			Bi-KP100			Bi-KP200		
WS-DP (101 pref.)	0.3563	0.83%	9.5m	0.4531	1.03%	1.2h	0.3599	2.20%	3.7h
PPLS/D-C (200 iter.)	0.3528	1.81%	18m	0.4480	2.14%	46m	0.3541	3.78%	1.4h
NSGAIL-KP	0.3112	13.39%	30m	0.3514	23.24%	31m	0.3511	4.59%	33m
EMNH	0.3561	0.89%	17s	0.4535	0.94%	53s	0.3603	2.09%	2.3m
DRL-MOA (101 models)	0.3559	0.95%	8s	0.4531	1.03%	13s	0.3601	2.15%	1.1m
PMOCO (101 pref.)	0.3552	1.14%	13s	0.4522	1.22%	19s	0.3595	2.31%	50s
NHDE-P (101 pref.)	<u>0.3564</u>	<u>0.81%</u>	1.1m	<u>0.4541</u>	<u>0.81%</u>	2.5m	<u>0.3612</u>	<u>1.85%</u>	5.3m
GAPL-alter (101 pref.)	<b>0.3593</b>	<b>0.00%</b>	21s	<b>0.4578</b>	<b>0.00%</b>	33s	<b>0.3680</b>	<b>0.00%</b>	1.4m
Method	Tri-TSP20			Tri-TSP50			Tri-TSP100		
WS-LKH (210 pref.)	0.4718	1.34%	20m	0.4493	2.30%	3.3h	0.5160	1.02%	11h
PPLS/D-C (200 iter.)	0.4698	1.76%	1.3h	0.4174	9.24%	3.8h	0.4376	16.06%	13h
NSGAIL-TSP	0.4216	11.84%	2.1h	0.4130	10.20%	2.3h	0.4291	17.69%	2.5h
DRL-MOA (1035 models)	0.4712	1.46%	51s	0.4396	4.41%	1.5s	0.4915	5.72%	3.1s
PMOCO (10201 pref.)	0.4749	0.69%	8.9m	0.4489	2.39%	17m	0.5102	2.13%	34m
NHDE-P (10201 pref.)	0.4764	0.38%	53m	0.4513	1.87%	1.8h	0.5118	1.82%	4.3h
GAPL-alter (10201 pref.)	0.4773	0.19%	10m	0.4517	1.78%	19m	0.5121	1.76%	41m
EMNH (aug.)	0.4712	1.46%	7.1m	0.4418	3.94%	58m	0.4973	4.60%	2.4h
PMOCO (10201 pref. & aug.)	0.4757	0.52%	20m	0.4573	0.57%	1.1h	0.5123	1.73%	4.3h
NHDE-P (10201 pref. & aug.)	<u>0.4772</u>	<u>0.21%</u>	2.1h	<u>0.4595</u>	<u>0.09%</u>	6.7h	<u>0.5210</u>	<u>0.06%</u>	15.3h
GAPL-alter (10201 pref. & aug.)	<b>0.4782</b>	<b>0.00%</b>	26m	<b>0.4599</b>	<b>0.00%</b>	1.3h	<b>0.5213</b>	<b>0.00%</b>	4.8h

## M.2 Generalization Study of GAPL and GAPL-alter

To assess the generalization capability of GAPL and GAPL-alter. We compare them with the other baselines on 200 random Bi-TSP instances with larger sizes, i.e., Bi-TSP150/200. The comparison results are demonstrated in Table 5. GAPL and GAPL-alter outperform the state-of-the-art MOEA (i.e., PPLS/D-C) and other neural methods significantly, in terms of HV, which means a superior generalization capability. Note that WS-LCK has a slight advantage over GAPL and GAPL-alter at the sacrifice of Dozens of times the inference time (i.e. 1.2 hours vs 4.6 minutes). Besides, GAPL is superior to GAPL-alter on both problems, which also Verifies our idea in Appendix M.1.

Table 5: Experimental results on 200 random instances for MOCO problems.

Type	Method	Bi-TSP150			Bi-TSP200		
		HV $\uparrow$	Gap $\downarrow$	Time $\downarrow$	HV $\uparrow$	Gap $\downarrow$	Time $\downarrow$
Traditional heuristics	WS-LKH (101 pref.)	<b>0.7075</b>	<b>-0.77%</b>	6.4h	<b>0.7435</b>	<b>-1.31%</b>	13h
	PPLS/D-C (200 iter.)	0.6784	3.38%	21h	0.7106	3.17%	32h
	NSGAII-TSP	0.6125	12.76%	2.1h	0.6318	13.91%	3.7h
Neural heuristics	DRL-MOA (101 models)	0.6901	1.71%	45s	0.7219	1.64%	2.1m
	PMOCO (101 pref.)	0.6912	1.55%	1.4m	0.7231	1.47%	3.1m
	NHDE-P (101 pref.)	0.6964	0.81%	12m	0.7280	0.80%	21m
	GAPL-alter (101 pref.)	0.6953	0.97%	2.3m	0.7273	0.90%	4.6m
	GAPL (101 pref.)	0.6972	0.70%	2.3m	0.7291	0.65%	4.6m
Neural heuristics augmentation	EMNH (aug.)	0.6983	0.54%	53m	0.7307	0.44%	2.9h
	PMOCO (101 pref. & aug.)	0.6967	0.77%	41m	0.7276	0.86%	2.9h
	NHDE-P (101 pref. & aug.)	0.7012	0.13%	1.3m	0.7324	0.20%	4.6h
	GAPL-alter (101 pref. & aug.)	0.7003	0.26%	53m	0.7316	0.31%	1.2h
	GAPL (101 pref. & aug.)	<u>0.7021</u>	<u>0.00%</u>	53m	<u>0.7339</u>	<u>0.00%</u>	1.2h

## M.3 Hyperparameter Studies

We further study the effects of  $P'$  (maximal size of polar angles pool) and  $c$  (control parameter of potential energy).

We present the results of various  $P'$  on Bi-TSP50 and Tri-TSP100 in Figure 6 (a) (b). As shown,  $P' = 5$  and  $P' = 10$  cause inferior performance, while proper  $P'$  ( $20 \leq P' \leq 40$ ) results in desirable performance. Intuitively, when limiting the same total gradient steps in training, a larger  $P'$  means fewer instances are used for model training. In this sense, too large  $P'$ , i.e., with insufficient instances, could lead to inferior performance for solving unseen instances. On the other hand, although the approximate HV is an unbiased estimation, when  $P'$  is too small, the calculated variance will become larger, which will also prevent the model from learning favorable global information and thus deteriorate the final performance. Hence we choose  $P' = 20$  in this paper.

Figure 6 (c) (d) displays the results of various values of  $c$ . As has been presented in Section 4.4, the potential energy function is as Eq. 6,  $c$  is a parameter that influences the result Former literature [51] has reported that  $c$  is a weak parameter, because the result does not change a lot when  $c$  varies, and the selection of this parameter is only related to the dimension of the objective space. In this part, an experiment is conducted to study the influence of  $c$  on Bi-TSP50 and Tri-TSP100 in Figure 6 (c) (d), the results also support the proposition of former researches. So, in this paper, we recommend to use  $c = 2m$  in LSS.

## M.4 More Geometric Visualization Results for Validity of Geometric Adaptation

We have shown visualization Results of all three classic MOCO problems for each decomposition method in Figure 7. All results can support the conclusion in Section 5.3 to reflect the superiority of GAPL’s geometric adaptation.

## N Convergence of the Pareto Front Hypervolume

Assuming that  $b \leq r_1 - y_i \leq B, \forall i \in \{1, \dots, m\}, y \in Y$ . Let  $\mathcal{Z}(\theta) = \frac{\Phi}{m2^m} \mathcal{V}_{\mathcal{X}}(\theta)^m$ , then  $\sup_{\theta} \mathcal{Z}(\theta) \leq \frac{\Phi}{m2^m} B^m m^{m/2}$ . Let  $\hat{\mathcal{H}}\mathcal{V}_r(Y) := \frac{1}{P} \sum_{i=1}^P \mathcal{Z}(\theta^{(i)})$  denote the empirical estimation of

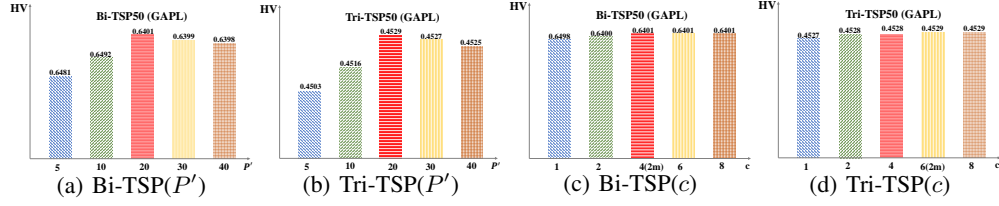


Figure 6: Hyperparameter study. (a) Effect of the maximal size of polar angles pool used in training on Bi-TSP50. (b) Effect of the maximal size of polar angles pool used in training on Tri-TSP100. (c) Effect of the control parameter of potential energy on Bi-TSP50. (d) Effect of the control parameter of potential energy on Tri-TSP50. points from new solutions for updating the Pareto front.

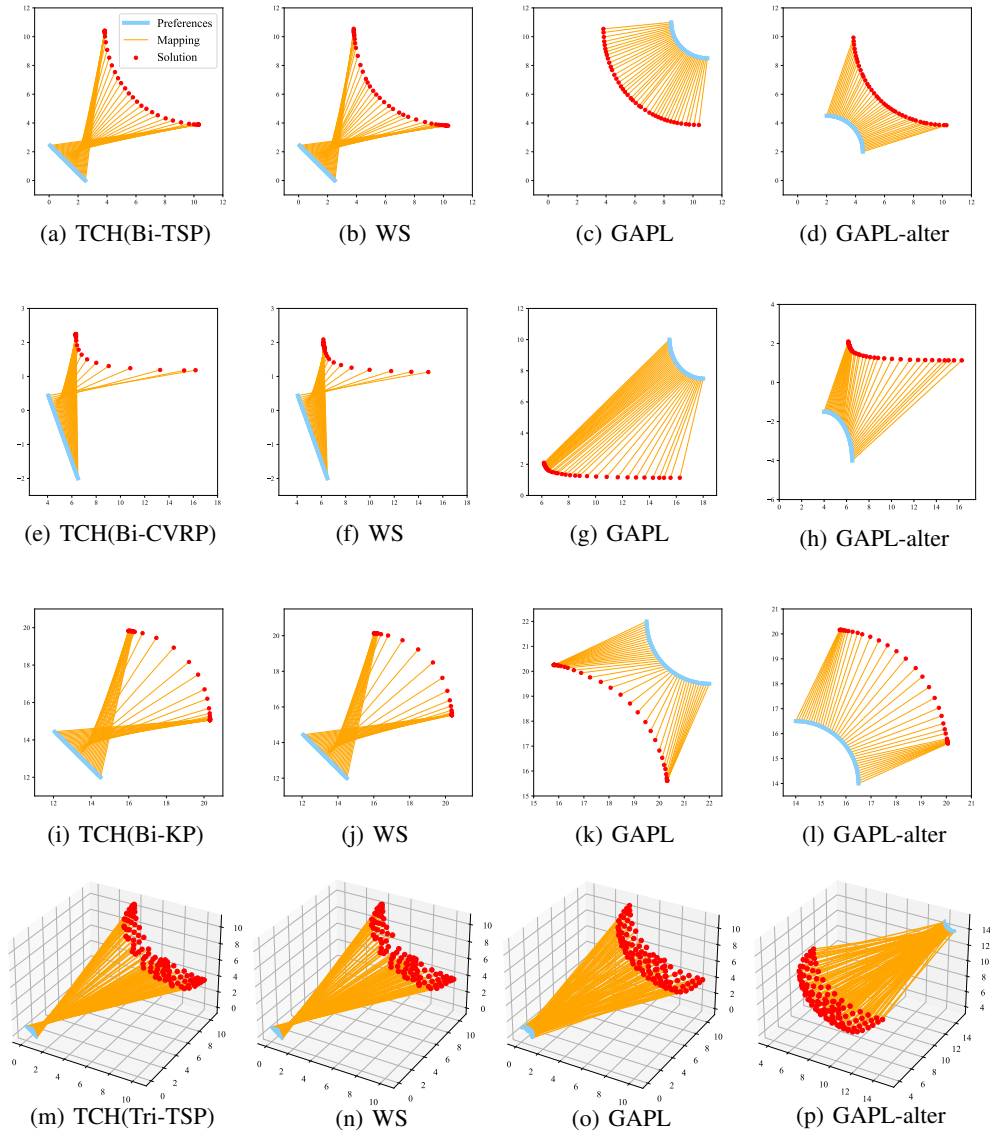


Figure 7: Visual comparisons on Bi-TSP20, Bi-CVRP, Bi-KP20 and Tri-TSP20. GAPL and GADL-alter have better adaptability than WS- and TCH-based approaches.

$\mathcal{H}\mathcal{V}_r(Y)$  with  $P$  samples. Via Hoeffding inequality, similar to [13], we have the following inequality:

$$\Pr(|\mathcal{H}\hat{\mathcal{V}}_r(Y) - \mathcal{H}\mathcal{V}_r(Y)| \geq \epsilon) \leq 2\exp\left(\frac{-P\epsilon^2 2^{m+2}}{\Phi^2 B^2 m^{m-2}}\right). \quad (30)$$

## O The bound of $\mathcal{V}_{\mathcal{X}}(\theta)$ in Eq. 10

Since  $\mathcal{V}_{\mathcal{X}}(\theta)$  is a max-min problem, we can conclude that the following inequalities hold:

$$\mathcal{V}_{\mathcal{X}}(\theta) \leq Bm^{\frac{1}{2}}, \quad (31)$$

where  $b \leq (r_i - f_i(\mathbf{x})) \leq B, \forall \mathbf{x} \in \mathcal{X}, \forall i \in \{1, \dots, m\}$  and  $\|\boldsymbol{\lambda}\|_2 = 1$ .

*Proof.*

$$\begin{aligned} \mathcal{V}_{\mathcal{X}}(\theta) &\leq \max_{\mathbf{x} \in \mathcal{X}, \|\boldsymbol{\lambda}\|_2=1} \left( \min_{i \in \{1, \dots, m\}} \left\{ \frac{r_i - f_i(\mathbf{x})}{\lambda_i(\theta)} \right\} \right) \\ &\quad (r_i - f_i(\mathbf{x}) \leq B) \\ &\leq \max_{\|\boldsymbol{\lambda}\|_2=1} \left( \min_{i \in \{1, \dots, m\}} \left\{ \frac{B}{\lambda_i(\theta)} \right\} \right) \\ &\leq \frac{B}{m^{-\frac{1}{2}}} \\ &= Bm^{\frac{1}{2}}. \end{aligned} \quad (32)$$

The transition from line one to line two is due to the fact that the inequality  $r_i - f_i(\mathbf{x}) \leq B$  holds for  $\forall \mathbf{x} \in \mathcal{X}$  and for  $\forall i \in \{1, \dots, m\}$ . The transition from line two to line three is  $\max_{\|\boldsymbol{\lambda}\|_2=1} \left( \min_{i \in \{1, \dots, m\}} \left\{ \frac{B}{\lambda_i(\theta)} \right\} \right)$  is an optimization problem under the constraint  $\|\boldsymbol{\lambda}\|_2 = 1$ . The upper bound for this optimization is when  $\lambda_1 = \dots = \lambda_m = m^{-\frac{1}{2}}$ .  $\square$

## P Equivalence of Hypervolume Calculation in Polar Coordinates

*Proof.*  $\mathcal{H}\mathcal{V}_r(Y)$  can be simplified by the following equations. Here  $\Omega$  denoted the dominated regions by the Pareto front, i.e.,  $\mathcal{H}\mathcal{V}_r(Y) = \Lambda(\Omega, \mathbf{r})$ .

$$\begin{aligned} \mathcal{H}\mathcal{V}_r(Y) &= \int_{\mathcal{R}^m} I_{\Omega} dy_1 \dots y_m \\ &\quad (\text{"}dv\text{" denoted the infinitesimal sector area.}) \\ &= \underbrace{\int_0^{\frac{\pi}{2}} \dots \int_0^{\frac{\pi}{2}}}_{m-1} dv \\ &\quad (\text{"}d\text{" equals the angle ratio multiplied by } \mathcal{V}_{\mathcal{X}}(\theta)^m \text{ multiplied by the unit for volume.}) \\ &= \underbrace{\int_0^{\frac{\pi}{2}} \dots \int_0^{\frac{\pi}{2}}}_{m-1} \frac{\Phi}{m} \cdot \frac{\mathcal{V}_{\mathcal{X}}(\theta)^m}{2\pi \cdot \pi^{m-2}} \underbrace{d\theta_1 \dots \theta_{m-1}}_{d\theta} \\ &= \frac{\Phi}{2m\pi^{m-1}} \underbrace{\int_0^{\frac{\pi}{2}} \dots \int_0^{\frac{\pi}{2}}}_{m-1} \mathcal{V}_{\mathcal{X}}(\theta)^m d\theta \\ &= \frac{\Phi}{2m\pi^{m-1}} \cdot \frac{\pi^{m-1}}{2} \cdot \mathbb{E}_{\theta}[\mathcal{V}_{\mathcal{X}}(\theta)^m] \\ &= \frac{\Phi}{m2^m} [\mathcal{V}_{\mathcal{X}}(\theta)^m]. \end{aligned} \quad (33)$$

We specify  $\theta \sim \text{Unif}(\Theta) = \text{Unif}([0, \frac{\pi}{2}]^{m-1})$  in Eq. 33.

Line 2 holds since it represents the integral of  $\Omega$  expressed in polar coordinates, where in the element  $dv$  corresponds to the volume associated with a segment obtained by varying  $d\theta$ .

Line 3 calculates the infinitesimal volume of  $dv$  by noticing the fact that the ratio of  $dv$  to  $\frac{\Phi}{m}$  is  $\frac{V_X(\theta)^m}{2\pi \cdot \pi^{m-2}}$ . Line 4 is a simplification of Line 3. And Line 5 and 6 express the integral in its expectation form.  $\square$

## Q Licenses

The licenses for the codes we used in this work are shown in Table 6.

Table 6: List of licenses for the codes suite we used in this work.

Resources	Type	Link	License
PSL-MOCO [8]	Code	<a href="https://github.com/Xi-L/PMOCO">https://github.com/Xi-L/PMOCO</a>	MIT License
NHDE [10]	Code	<a href="https://github.com/Bill-CJB/NHDE">https://github.com/Bill-CJB/NHDE</a>	MIT License
EMNH [29]	Code	<a href="https://github.com/Bill-CJB/EMNH">https://github.com/Bill-CJB/EMNH</a>	MIT License